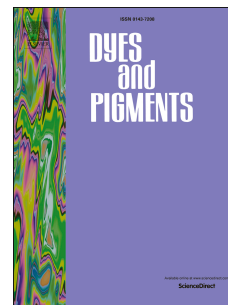


Accepted Manuscript

Low-temperature nematic phase in azo functionalised reactive hockey stick mesogens possessing lateral methyl group

Manoj Kumar Paul, Sandip Kumar Saha, Gayatri Kalita, Barnali Bhattacharya, Utpal Sarkar



PII: S0143-7208(18)32109-0

DOI: <https://doi.org/10.1016/j.dyepig.2018.12.028>

Reference: DYPI 7233

To appear in: *Dyes and Pigments*

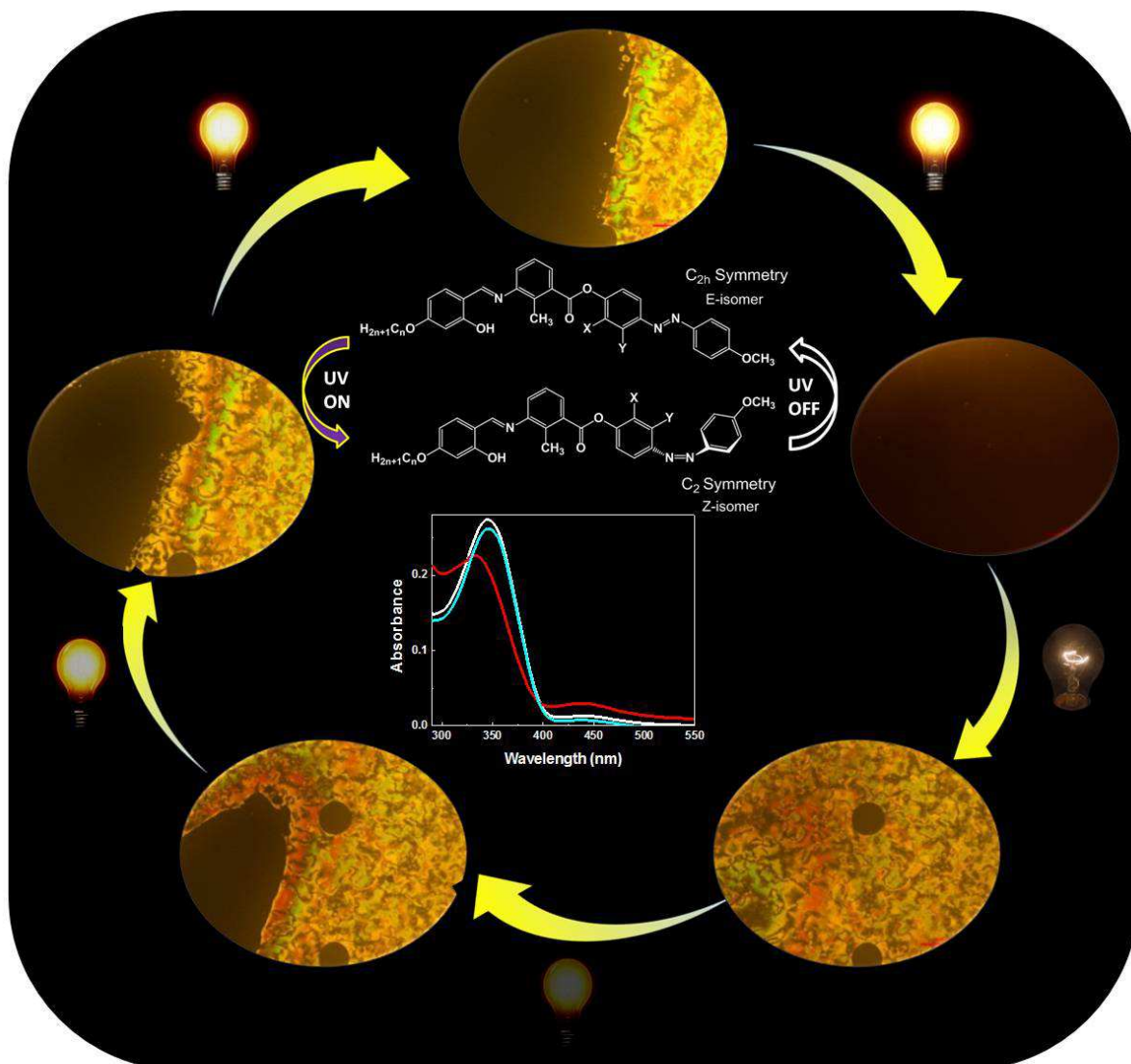
Received Date: 22 September 2018

Revised Date: 14 December 2018

Accepted Date: 16 December 2018

Please cite this article as: Paul MK, Saha SK, Kalita G, Bhattacharya B, Sarkar U, Low-temperature nematic phase in azo functionalised reactive hockey stick mesogens possessing lateral methyl group, *Dyes and Pigments* (2019), doi: <https://doi.org/10.1016/j.dyepig.2018.12.028>.

This is a PDF file of an unedited manuscript that has been accepted for publication. As a service to our customers we are providing this early version of the manuscript. The manuscript will undergo copyediting, typesetting, and review of the resulting proof before it is published in its final form. Please note that during the production process errors may be discovered which could affect the content, and all legal disclaimers that apply to the journal pertain.



Low-temperature nematic phase in azo functionalised reactive hockey stick mesogens possessing lateral methyl group

Manoj Kumar Paul*¹, Sandip Kumar Saha¹, Gayatri Kalita¹, Barnali Bhattacharya² and Utpal Sarkar²

¹Department of Chemistry, Assam University, Silchar-788011 (India)

²Department of Physics, Assam University, Silchar-788011 (India)

Email: paulmanojaus@gmail.com

Abstract

We report, the design, synthesis and mesomorphic behaviour of new hockey stick mesogens containing photochromic azo group and a reactive double bond. The structure of the compounds resemble the hockey stick due to unequal distribution of the phenyl rings in the two arms of the molecule and possess a reactive 4-*n*-undecenyloxy chain attached at short arm of the bent-core molecule, while the elongated arm consists of a small methoxy group and photochromic azo linkage between two phenyl rings. All the compounds exhibit a wide-range of enantiotropic nematic phase at low temperature. The photo-responsive behaviour of nematic phase was characterized by polarizing optical microscopy with *in situ* white light irradiation. Upon irradiation, the nematic phase almost completely disappeared in about 20s. We have also investigated the effect of the position of methyl group substitution at the outer phenyl ring of the elongated arm of the molecule on the nematic phase of azo functionalised compounds. Our theoretical calculations predict that different position of methyl group does not bring any significant change in reactivity profile, electronic properties and spectroscopic properties. Irrespective of the position of a methyl group, *trans* conformation has slightly greater stability as well as less reactivity than *cis* conformation.

Keywords: Azo-functionalised mesogen; bent-core mesogens; reactive mesogens; a nematic phase

1. Introduction

Azo-functionalised materials are one of the attractive classes of the functional materials due to their interesting photoswitching behaviour and have diverse potential applications *viz.*, optical data storage, display devices, molecular switches, nonlinear optical devices, photomechanical systems [1-8]. In recent years, azo functionalised mesogenic materials have generated a lot of interest due to the great demand for new multifaceted functional and smart materials. Azo functionalised mesogenic materials have the dual properties of azobenzene (*viz.*, photoswitching behaviour) and mesogens (*viz.*, anisotropy and fluidity) which in turn generate unique photo-induced anisotropy and photo-chemical phase transitions [9-14]. In order to understand their rich mesomorphic behaviour and their multifaceted properties, a large number of the azo functionalised bent-core mesogens (BCMs) have been designed, synthesised, their mesomorphic behaviours were characterized and structure-property relationships were recently studied by several research groups [15-19] and are well documented in excellent review published recently [20]. Mesogens containing olefinic chain can generate new functional mesogens because of their low viscosity, low melting point, high clearing points and good low-temperature stability [21]. In addition, the double bond in an olefinic chain is reactive and can be used to prepare mesogenic polymers [22-24] and elastomers [25-26]. The photochromic azobenzene mesogens containing a reactive double bond were reported in the past decade [27-29]. Since the discovery of macroscopic polar order and chiral superstructure in the mesophase of achiral bent-core mesogens (BCMs) is a well-established subclass of thermotropic mesogens [30-35]. The mesophases (*viz.*, B₁-B₈) displayed by the BCMs are different from the rod-shaped mesogens in term of their physical properties and their fascinating optical textures (B₁-B₇). However, some of the BCMs exhibited similar phases as displayed by the rod-like mesogens. Interestingly of these, nematic phase exhibited by the bent-core mesogens drags special attention and one of the active topics of debate due to their unusual physical properties like huge flexoelectricity[36], unusual dielectric relaxation [37], unusual electro-convection pattern [38], magnetic field induced birefringence [39] and interestingly ferro-nematics [37,40]. The unusual physical properties of the nematic phase exhibited by the bent-core mesogens which are expected due to the presence of nanometer-sized polar smectic clusters in the nematic phase so-called cybotactic nematic phase [41-46]. The formation of the nanometer-sized polar smectic cluster in the nematic phase of bent-core systems may be due to kink geometry of the molecules which restricts the free

rotation and core-core interactions between the molecules promotes the layer formation due to the segregation between extended aromatic moieties and end alkyl chains along the orientational direction of the long axes. Moreover, over four decades back, theoretically, it was predicted that the shape anisotropy of the low molar mass bent-core molecule is an ideal criterion for the biaxiality in the nematic phase. The biaxial nematic phase has an advantage over uniaxial nematic phase due to fast switching response and has potential application in the new generation of ultrafast and wide-angle display devices. Since then, researchers have made several attempts to design and synthesized new BCMs exhibiting nematic phase and claimed biaxiality in the nematic phase and result ended without success [20, 47-48]. In the recent years, four ring bent-core mesogens so-called hockey stick shaped mesogens have attracted considerable attention due to their rich mesomorphism [49-52]. Interestingly, it is noted from the literature that most of the hockey stick molecules containing azo linkage exhibit nematic phase [53-57]. Hockey stick shaped mesogens containing functionalised azo-benzene moiety are sensitive to light [58] due to photo-isomerization *i.e.*, *cis* (Z-isomer) to *trans* (E-isomer) isomer which change the geometry of the molecule further lead to a concomitant change in chemical and physical properties of the molecules. Therefore, in order to understand how such structural modifications impact the mesomorphic behaviour, we designed four ring hockey stick shaped molecule consist of three linking groups (-N=N-, -COO- and -CH=N-) connecting the phenyl rings and lateral methyl group as a substituent at the elongated arm of the molecule. In particular, the position of the methyl group would yield further reduced nematic onset temperatures without exclusion of mesomorphism [59]. We report here the synthesis and phase characterization of azo functionalised reactive hockey stick mesogens and study the influence of lateral methyl substitution on mesomorphic behaviour, photoswitching and their reactivity.

Experimental

The chemicals used for the synthesis of the hockey stick compounds were procured from M/s Alfa Aesar or Aldrich or Tokyo Kasei Kogyo Co. Ltd. The solvents and reagents are of analytical reagent grade and were distilled and dried before use. Elemental analysis was performed on Carlo-Erba 1106 elemental analyzer. FT-IR spectra were recorded on a Shimadzu IR Prestige-21 over the 400-4000 cm^{-1} spectral range in KBr pellets. The ^1H NMR spectra were recorded in CDCl_3 solution either on JEOL AL300 FTNMR multinuclear spectrometer or Bruker

Avance III-400 spectrometer (chemical shift δ in parts per million relative to tetramethylsilane (TMS) as internal standard). UV-visible absorption spectra of the compounds in dichloromethane were recorded on Perkin-Elmer Lambda 35 spectrophotometer. *Trans-cis* photo-isomerization was performed *in situ* in an experimental setup assembled with the white halogen lamp. The phase transition temperatures, associated enthalpies and entropies were recorded at a heating and cooling rate of $5\text{ }^{\circ}\text{Cmin}^{-1}$ using differential scanning calorimetry (DSC) (Perkin-Elmer Pyris1 system). The DSC was calibrated with indium ($156.6\text{ }^{\circ}\text{C}$, 28.4 Jg^{-1}) and tin ($232.1\text{ }^{\circ}\text{C}$, 60.5 Jg^{-1}). The liquid crystalline properties of the compounds were characterized using a polarizing optical microscope (POM) (Nikon optiphot-2-pol attached with hot and cold stage HCS302, with STC200 temperature controller configured for HCS302 from INSTRON Inc. USA).

The detailed synthesis of the intermediate compounds *viz.*, 4-*n*-undecenyloxy-2-hydroxybenzaldehyde (**1**), 3-amino-2-methyl benzoic acid (**2**), 2-Methyl-3-N-(4-*n*-undecenyloxysalicylidene) aminobenzoic acid (**3**) was prepared following the earlier reported procedures [55].

Synthesis of 4-hydroxy-4'-methoxy azobenzene (4a)

4-Hydroxy-4'-methoxy azobenzene was prepared following the general procedure reported earlier [55, 60-61]. 4-methoxyaniline (2.46g, 20 mmol) were added 10 mL of distilled water containing hydrochloric acid (12M, 2.5 mL, 30 mmol) and the mixture was stir and warm to dissolve completely. The solution was then cooled down to 0°C ice bath. To this ice-cold solution, a freshly prepared sodium nitrite solution (2.34g, 33 mmol) was added with stirring keeping the temperature in between $0-5\text{ }^{\circ}\text{C}$. The resulting diazonium chloride was consecutively coupled with an alkaline solution of phenol (1.88g, 20mmol) with constant stirring. The reaction mixture was neutralized (pH= 7) by an aqueous solution of Na_2CO_3 and was allowed to attain room temperature. The azo dye which formed immediately as a yellow precipitate was filtered, washed several times with distilled water and dissolved in diethyl ether, and the resulting organic solution dried over anhydrous sodium sulphate. The crude product obtained after removal of the solvent under reduced pressure was purified by recrystallization from cold hexane. The precipitate was filtered and washed with water and methanol and dried in vacuum to yield yellow solid. m.p.: 139°C , Yield = 3.2g (70 %). FT-IR ν_{max} in cm^{-1} : 3421 ($\nu_{\text{O-H}}$), 1467 ($\nu_{\text{N=N}}$, azo). ^1H NMR (CDCl_3 , 300MHz): (δ in ppm) 7.87 (d, 2H, J = 8.7Hz, ArH), 7.82 (d, 2H, J = 8.4Hz, ArH),

6.92 (d, 2H, J = 7.8Hz, ArH), 6.70 (d, 2H, J = 8.4Hz, ArH), 5.44 (s, 1H, -OH), 3.87 (s, 3H, -OCH₃). Elemental analysis calculated for C₁₃H₁₂N₂O₂: C, 68.41; H, 5.30; N, 12.27%. Found: C, 68.02; H, 5.23; N, 12.31 %.

Synthesis of 4-hydroxy-2-methyl-4'-methoxy azobenzene (4b)

2-Methyl-4-hydroxy-4'-methoxy azobenzene was synthesized following the same procedure described for the synthesis of **4a**. Starting material 4-*n*-methoxyaniline (2.46g, 20mmol), hydrochloric acid (12M, 2.5mL, 30mmol), sodium nitrite (2.34g, 33mmol), *o*-cresol (2.16g, 20mmol), the crude product obtained after removal of the solvent under reduced pressure was purified by recrystallization from cold hexane. The precipitate was filtered and washed with water and methanol and dried in vacuum to yield yellow solid. m.p.: 147 °C, Yield = 3.1g (64.04 %). FT-IR ν_{\max} in cm⁻¹: 3163 ($\nu_{\text{O-H}}$), 1462 ($\nu_{\text{N=N}}$, azo). ¹H NMR (CDCl₃, 300MHz): (δ in ppm): (d, 2H, J = 9.0Hz, ArH), 7.66 (d, 2H, J = 8.7Hz, ArH), 6.98 (d, 2H, J = 9.0Hz, ArH), 6.86 (d, 1H, J = 8.4Hz, ArH), 5.25 (s, 1H, -OH), 3.86 (s, 3H, -OCH₃), 2.31 (s, 3H, Ar-CH₃). Elemental analysis calculated for C₁₄H₁₄N₂O₂: C, 69.41; H, 5.82; N, 11.56 % Found: C, 69.43; H, 5.81; N, 11.67 %.

Synthesis of 4-hydroxy-3-methyl-4'-methoxy azobenzene (4c)

3-Methyl-4-hydroxy-4'-methoxy azobenzene was synthesized following the same procedure described for the synthesis of **4a**. Starting material 4-*n*-methoxyaniline (2.46g, 20mmol), hydrochloric acid (12 M, 2.5mL, 30mmol), sodium nitrite (2.34g, 33mmol), *m*-cresol (2.16g, 20mmol), the crude product obtained after removal of the solvent under reduced pressure was purified by recrystallization from cold hexane, precipitate was filtered and washed with water and methanol and dried in vacuum to yield yellow solid. m.p.: 131 °C, Yield = 3.4g (70.39 %). FT-IR ν_{\max} in cm⁻¹: 3143 ($\nu_{\text{O-H}}$), 1433 ($\nu_{\text{N=N}}$, azo). ¹H NMR (CDCl₃, 300MHz): (δ in ppm) (d, 2H, J = 9.0Hz, ArH), 7.68 (d, 2H, J = 8.1Hz, ArH), 7.66 (d, 2H, J = 8.4Hz, ArH), 6.84 (d, 1H, J = 8.4Hz, ArH), 5.15 (s, 1H, -OH), 3.86 (s, 3H, -OCH₃), 2.34 (s, 3H, Ar-CH₃). Elemental analysis calculated for C₁₄H₁₄N₂O₂: C, 69.41; H, 5.82; N, 11.56%. Found: C, 69.52%; H, 5.80%; N, 11.67 %.

General procedure for the synthesis of azo-functionalised reactive hockey stick shaped compounds

Appropriate quantity of substituted 4-hydroxy-4'-methoxy azobenzene (*viz.*, 4-hydroxy-4'-methoxy azobenzene (**4a**), 0.46g; 4-hydroxy-2-methyl-4'-methoxy azobenzene (**4b**) 0.48g; 4-

hydroxy-3-methyl-4'-methoxy azobenzene (**4c**) 0.48g, (2.0 mmol) and 2-methyl-3-N-(4-*n*-undecenyloxy-2-hydroxybenzylidene) aminobenzoic acid (**3**) (0.65 g, 2.0 mmol) and was dissolved in dry dichloromethane (DCM) (50mL) and catalytic amount of 4-dimethylaminopyridine (DMAP) (4 mg, 0.02 mmol) was added to the solution. A solution of N, N'-dicyclohexylcarbodiimide (DCC) (0.49 g, 2.4 mmol) was added to the reaction mixture and the mixture was stirred for 48 h under the nitrogen atmosphere at room temperature. The precipitate of N, N'-dicyclohexylurea was removed by filtration and the solvent DCM was evaporated to get crude product. The crude product was purified by column chromatography using silica gel (60-120 mesh) with hexane/ chloroform (9:1) as eluent. The yellow solid was recrystallized several times from absolute ethanol to get the pure product.

(4'-methoxy phenyl azo) phenyl-4-yl 3-[N-(4'-*n*-undecenyloxy-2-hydroxybenzylidene)amino]-2-methyl benzoate (5a).

Yellow solid, Yield: 0.71 g (73 %). FT-IR ν_{\max} in cm^{-1} : 3192 ($\nu_{\text{O-H}}$ H-bonded); 1741 ($\nu_{\text{C=O}}$, ester); 1610 ($\nu_{\text{C=N}}$, imine). ^1H NMR (400 MHz, CDCl_3): (δ in ppm) 13.44 (s, 1H, -OH); 8.38 (s, 1H, -CH=N-); 7.93 (d, 2H, J = 6.8 Hz, ArH); 7.86 (d, 2H, J = 8.8 Hz, ArH); 7.30 (d, 2H, J = 8.4 Hz, ArH); 7.19-7.24(m, 4H, ArH); 6.89 (d, 2H, J = 8.4 Hz, ArH); 6.45 (s, 2H, ArH); 5.71-5.75(m, 1H, -CH=); 4.85-4.95 (m, 2H, =CH₂); 3.94 (t, 2H, J = 6.4 Hz, -OCH₂-); 3.83 (s, 3H, -OCH₃); 2.61 (s, 3H, -CH₃); 1.96-1.98 (m, 2H, -OCH₂-CH₂-); 1.71-1.75 (m, 2H, -OCH₂-CH₂-CH₂-); 1.24-1.39 (m, 12H, 6x-CH₂-). Elemental analysis calculated for C₃₉H₄₃N₃O₅: C, 73.91; H, 6.84; N, 6.63 %. Found: C, 73.87; H, 6.86; N, 6.61%.

(4'-methoxy phenyl azo) phenyl-4-yl 3-[N-(4'-*n*-undecenyloxy-2-hydroxybenzylidene)amino]-2-methyl benzoate (5b).

Yellow solid, Yield: 0.74 g (75 %). FT-IR ν_{\max} in cm^{-1} : 3192 ($\nu_{\text{O-H}}$ H-bonded); 1741 ($\nu_{\text{C=O}}$, ester); 1610 ($\nu_{\text{C=N}}$, imine). ^1H NMR (400 MHz, CDCl_3): (δ in ppm) 13.51 (s, 1H, -OH); 8.45 (s, 1H, -CH=N-); 8.03 (d, 1H, J = 7.6 Hz, ArH); 7.92 (d, 2H, J = 8.8 Hz, ArH); 7.82 (d, 2H, J = 9.2 Hz, ArH); 7.26-7.41 (m, 4H, ArH); 7.02 (d, 2H, J = 8.4 Hz, ArH); 6.52 (s, 2H, ArH); 5.78-5.85(m, 1H, -CH=); 4.92-5.02 (m, 2H, =CH₂); 4.01 (t, 2H, J = 6.2 Hz, -OCH₂-); 3.90 (s, 3H, -OCH₃); 2.69 (s, 3H, -CH₃); 2.36 (s, 3H, -CH₃); 2.02-2.07 (m, 2H, -OCH₂-CH₂-); 1.77-1.84 (m, 2H, -OCH₂-CH₂-CH₂-); 1.25-1.46 (m, 12H, 6x-CH₂-). Elemental Analysis calculated for C₄₀H₄₅N₃O₅: C, 74.16; H, 7.00; N, 6.49%. Found: C, 74.27; H, 6.95; N, 6.43%.

(4'-methoxy phenyl azo) phenyl-4-yl 3-[N-(4'-*n*-undecenyloxy-2-hydroxybenzylidene)amino]-2-methyl benzoate (**5c**).

Yellow solid, Yield: 0.76 g (77 %). FT-IR ν_{\max} in cm^{-1} : 3192 ($\nu_{\text{O-H}}$ H-bonded); 1741 ($\nu_{\text{C=O}}$, ester); 1610 ($\nu_{\text{C=N}}$, imine). ^1H NMR (400 MHz, CDCl_3): (δ in ppm) 13.52 (s, 1H, -OH); 8.44 (s, 1H, -CH=N-); 7.98 (d, 1H, $J = 7.6$ Hz, ArH); 7.93 (d, 2H, $J = 8.8$ Hz, ArH); 7.73 (d, 2H, $J = 8.4$ Hz, ArH); 7.21-7.39(m, 4H, ArH); 7.02 (d, 2H, $J = 8.4$ Hz, ArH); 6.51 (s, 2H, ArH); 5.78-5.85(m, 1H, -CH=); 4.92-5.02 (m, 2H, =CH₂); 4.01 (t, 2H, $J = 6.6$ Hz, -OCH₂-); 3.90 (s, 3H, -OCH₃); 2.74 (s, 3H, -CH₃); 2.65 (s, 3H, -CH₃); 2.02-2.07 (m, 2H, -OCH₂-CH₂-); 1.77-1.83 (m, 2H, -OCH₂-CH₂-CH₂-); 1.31-1.46 (m, 12H, 6x -CH₂-). Elemental Analysis calculated for $\text{C}_{40}\text{H}_{45}\text{N}_3\text{O}_5$: C, 74.16; H, 7.00; N, 6.49%. Found: C, 74.18; H, 6.97; N, 6.56%.

Results and Discussion

Design and Synthesis

New hockey stick shaped molecules possess two arms of a different number of phenyl rings. One arm consists of two phenyl rings and other have only one phenyl ring. The phenyl rings in the hockey stick shaped molecules are connected by three linkages *viz.*, imine linkage (-C=N-), an ester linkage (-COO-) and photochromic azo linkage (-N=N-). The hockey stick shaped molecule is considered as a subclass of unsymmetrical bent-core molecules with a bending angle is in the borderline between a typical bent shaped molecule and a conventional rod-shaped molecule. The short arm of the molecule possesses reactive 4-*n*-undecenyloxy moiety as a terminal chain while small methoxy moieties at the elongated end of the molecule. Further, asymmetry in a bent-core molecule is induced by the lateral methyl group at the outer phenyl ring of the elongated arm of the molecule. The position of the lateral methyl group is either in *ortho* position or *meta* position with respect to ester linking moieties. The presence of *ortho* hydroxyl group in benzylidene moiety enhances the stability of the imine through intramolecular H-bonding also enhances the transverse dipole-moment. The mesophase transition (nematic to isotropic transition) of these materials possessing a photochromic azo group can be induced by the *trans-to-cis* isomerization under the influence of UV irradiation [62]. The synthetic details of the azo-functionalised hockey stick mesogens compounds as described in **scheme 1** was carried out following the procedure described in the experimental section. The Williamson etherification of 2,4-dihydroxybenzaldehyde with 4-*n*-undecenylbromide preferentially takes

place at the *p*-hydroxyl group rather than the *o*-hydroxyl group which is involved in intramolecular hydrogen bonding with carbonyl oxygen atom [63-64], to form 4-*n*-undecenyloxy-2-hydroxy benzaldehyde (**1**). The 4-*n*-undecenyloxy-2-hydroxy benzaldehyde was then condensed with 3-amino-2-methyl benzoic acid (**2**) to yield 3-(4-*n*-undecenyloxy-2-hydroxybenzylidene)-2-methyl benzoic acid (**3**). The compound (**3**) was further esterified with 4-hydroxy-4'-methoxy azobenzene (**4a**) or substituted 4-hydroxy-4'-methoxy azobenzene (**4b** or **4c**) by DCC-DMAP reaction [65] to obtain the azofunctionalised hockey stick reactive mesogens (**5a-5c**). Elemental analyses of all the compounds were consistent with the proposed molecular structure and confirm the purity of the compounds. All the compounds were characterized by FT-IR and ¹H NMR studies. The infrared spectra of all the compounds exhibited characteristic peaks stretching vibration *ca.*1604-1612 cm⁻¹ indicates the formation of the Schiff base (-CH=N-) and the sharp peak ~1735 indicates the carbonyl (-C=O) stretching of the ester group. The weak broad peak ~3200-3250 indicates the -O-H stretching of the hydroxyl group involved in H-bonding. The phenolic C-O stretching vibration was observed around 1290 cm⁻¹. ¹H NMR spectra of the compounds showed a singlet appeared in the range of $\delta = 8.38-8.45$ ppm for imine (-HC=N-) proton of the compound, which confirmed the formation of the Schiff base. The lateral hydroxyl group appeared as a singlet in the range of $\delta = 13.44 -13.52$ ppm. All other aromatic protons appeared in the range of $\delta = 6.45-8.03$ ppm. The multiplets appeared for the terminal vinyl group the in $\delta = 4.85-5.02$ ppm as for =CH₂ protons and $\delta = 5.71-5.85$ ppm for -CH= proton. The NMR spectra of the target molecules are presented in ESI (**Fig. S1(a)-(c)**).

Mesomorphic behaviour

The mesomorphic behaviour of the new hockey stick shaped compounds is characterised by polarising optical microscopy (POM) and further confirmed by differential scanning calorimetry (DSC). The phase transition temperatures, transition enthalpy and entropy of the compounds are summarised in **Table 1**. It is observed from **Table 1** that all the azo functionalised hockey stick shaped compounds (**5a-5c**) exhibit a wide range of enantiotropic nematic phase. There is a distinct decrease in melting and clearing temperature on substitution at the outer phenyl ring of the elongated arm of the molecule. The temperature range of the nematic phase in a heating process decreases upon substitution with a methyl group at the elongated arm of the molecule whereas the nematic phase temperature window becomes broaden on cooling the sample. Therefore, the nematic phase becomes supercooled upon substituted with a methyl group at the

outer phenyl ring of the compounds. In the heating cycle, the compound (**5a**) exhibits two endothermic peaks that correspond to the two transitions such as Cr-N and N-Iso. The large change in enthalpy (41.88 kJmol^{-1}) and entropy ($105.7 \text{ Jmol}^{-1}\text{K}^{-1}$) value at $122.4 \text{ }^\circ\text{C}$ suggests the melting temperature of the compound and indicated the first order transition of order crystals to disorder nematic transition. On further heating, the sample at $161.8 \text{ }^\circ\text{C}$, a small change in enthalpy (0.33 kJmol^{-1}) and entropy ($0.76 \text{ Jmol}^{-1}\text{K}^{-1}$) during the transition indicating the weak first-order transition of nematic to an isotropic phase. In the cooling cycle, also two exothermic transition peaks were observed at $158.8 \text{ }^\circ\text{C}$ with a small change in enthalpy ($\Delta H = 0.27 \text{ kJmol}^{-1}$) indicated Iso-N transition. On further cooling, a second transition appeared at $78.4 \text{ }^\circ\text{C}$ with a large enthalpy change of 22.74 kJmol^{-1} indicating N-Cr transition presented in **Fig. 1**. The optical texture of the mesophase was analyzed by sandwiched the sample in between the untreated glass plates and coverslip. The compound **5a**, on cooling from the isotropic liquids, exhibited schlieren textures with two brush defects ($s=\pm 1/2$) and four brush defects ($s=\pm 1$), a characteristic of the nematic phase as presented in **Fig. 2(a)**. It is interesting to note that the optical texture of the nematic phase consists of a large number of the two brush defects which is quite unusual in the rod-shaped mesogens [66-67]. Similar behaviour of the nematic phase reported in the four ring bent-core mesogens [69]. Further, the presence of the homeotropic domains in the optical texture of the nematic phase and low enthalpy change during Iso-N transition indicating the formation of the cybotactic cluster which is commonly observed in nematic phases exhibited by bent-core compounds [37, 52, 69]. The sample, on further cooling, two brush schlieren texture with homeotropic domains of compound (**5a**) transform to a crystalline phase at $78.4 \text{ }^\circ\text{C}$ as presented in **Fig. 2(b)**. Similar phase behaviour observed in a methyl substituted hockey stick molecules (**5b** and **5c**). In an *ortho*-methyl substituted compound (**5b**) exhibits enantiotropic nematic phase. In the heating cycle, the compound **5b** also exhibits two endothermic peaks corresponds to Cr-N and N-Iso transition. The Cr-N transition occurs at $117.4 \text{ }^\circ\text{C}$ corresponds to the large change in enthalpy ($\Delta H=42.69 \text{ kJmol}^{-1}$) and entropy ($\Delta S=109.34 \text{ Jmol}^{-1}\text{K}^{-1}$) which indicate the first order transition whereas peak observed at $128.2 \text{ }^\circ\text{C}$ corresponds to N-Iso transition with a small change in enthalpy ($\Delta H=0.14 \text{ kJmol}^{-1}$), and entropy ($\Delta S=0.35 \text{ Jmol}^{-1}\text{K}^{-1}$) during the transition. In the cooling cycle, one peak is observed at $126.9 \text{ }^\circ\text{C}$ with the small change in enthalpy ($\Delta H=0.36 \text{ kJmol}^{-1}$), and entropy ($\Delta S=1.39 \text{ Jmol}^{-1}\text{K}^{-1}$) corresponds to Iso-N transition. The lower value of entropy during the

isotropic-nematic transition for these hockey stick molecules can be accounted for enhanced molecular biaxiality [70]. The N-Cr transition was not detected in the cooling cycle (see **Fig.3**). On slow cooling, the compound (**5b**) from an isotropic liquid, schlieren textures with two and four brush defects observed (see **Fig. 4a**) which on further cooling transforms to homeotropic texture (see **Fig. 4b**) indicates the formation of the cybotactic cluster in the nematic phase. On further cooling, the thread like texture appeared from dark homeotropic texture (see **Fig. 4c-d**) and finally crystallization occurs at 54.9 °C (see **Fig. 4e**) which was not observed by DSC. Similar behaviour was also observed for the compound (**5c**). The optical texture and the DSC thermogram is presented in the ESI **Fig. S2 and Fig. S3**. The substitution of the lateral bulky methyl group in a hockey stick shaped molecule decreases the melting and isotropic temperature without changing the mesophase. Further, it is interesting to note that the position of the lateral bulky methyl group plays an important role in the thermal stability of the compound. The substitution of the methyl group in the *meta*-position of the ester linkage decrease the nematic phase to room temperature whereas, the substitution of a methyl group at *ortho*-position of the ester linkage decrease the nematic phase to low temperature as compared to non-substituted compound (**5a**).

Photo-isomerization study

In solution

The azobenzene hockey stick compounds (**5a-5c**) are interesting dynamic functionalised materials because of their *trans-cis* or *cis-trans* isomerisation processes due to external stimuli *viz.*, irradiation by UV light, mechanical stress, electrostatic stimulation or recovering the thermodynamic stability. The photoswitching properties of all the hockey stick compounds were performed in chloroform ($c = 1 \times 10^{-5}$ M) using UV-visible absorption spectrometer. The UV-visible absorption spectra of compounds (**5a-5c**) are presented in **Fig. 5** and **Table 2**. It shows that strong absorption in the UV region ~ 346 nm with a large molar extinction coefficient ($\epsilon = 27038-28711 \text{ Lmol}^{-1}\text{cm}^{-1}$), which reflected the symmetry allowed $\pi-\pi^*$ transition of *trans* isomer of the azobenzene chromophore. However, a weak absorption in the visible region ~ 438 nm ($\epsilon \sim 1346-1574 \text{ Lmol}^{-1}\text{cm}^{-1}$) corresponding to symmetry forbidden $n-\pi^*$ transition of *cis* isomer. It is interesting to note that the substitution of the methyl group at the different position with respect to azo and /or ester group in the bent-core mesogens did not change the electronic structure of the molecule. Therefore, the UV-visible absorption spectra of the compounds are

almost similar. The UV-visible absorption spectra of representative compound **5c** shown in **Fig. 6** were obtained in 1×10^{-5} M solution in CHCl_3 at three different conditions *viz.*, (a) virgin sample solution, (b) solution after exposure to UV light (366 nm) for 30 mins and (c) solution kept in dark for 24 h. It is noted that there is a change in the molar extinction coefficient (ϵ) of the absorption band and peak positions of each compound from virgin sample solution to UV light irradiated solution and solution kept in dark for 24h. The absorption bands at 346 nm ($\epsilon = 27349 \text{ Lmol}^{-1}\text{cm}^{-1}$) and ~ 438 nm ($\epsilon = 1346 \text{ Lmol}^{-1}\text{cm}^{-1}$) are due to the π - π^* and n - π^* electronic transitions, respectively. The freshly prepared dilute solution of the compounds when irradiated with UV light (366 nm) for 30 minutes, the resulting UV-visible spectra illustrated that the π - π^* transition band is blue shifted (~ 10 - 12 nm) with a decrease in molar extinction coefficient (ϵ) of the band for the compound (**Fig. 6(b)**). This is due to the fact that before the irradiation with the UV light, the hockey stick shaped molecules are in *trans* (E-isomer) conformation with respect to the azo (-N=N-) group and upon absorption of photon by the irradiation with the UV light, the *trans* conformation flips to *cis* conformation (Z-isomer) with respect to the azo (-N=N-) group. This, in turn, leads to the breaking down of the symmetry C_2 for *trans* (E-isomer) conformation to C_{2h} for the *cis* (Z-isomer) conformation, indicating a less conjugation. Therefore, after UV irradiation π - π^* band shift towards the lower wavelength. However, the opposite phenomenon occurred in the case of n - π^* transition band. The molar extinction coefficient (ϵ) of the n - π^* band of the freshly prepared solution, *i.e.*, the virgin solution is less than solution irradiated with UV light. The increase in the molar extinction coefficient (ϵ) of the n - π^* absorption band is the transformation of the symmetry of the molecule from *trans* to *cis* isomer. When the solution was kept in dark for 24h, the position of the π - π^* and n - π^* bands were gradually shifted and the UV-visible absorption spectra appeared closer to the UV-visible absorption spectra of the virgin solution which confirms reversible photo-switching behaviour (**Fig. 6(c)**). The similar behavior is observed for the compounds **5a** and **5b** as presented in ESI **Fig. S4** and **Fig. S5**, respectively.

In Liquid Crystalline thin film

The effect of *trans*-to-*cis* photoisomerization caused by the UV irradiation on the nematic phase exhibited by the compounds was investigated. The nematic phase exhibited by the hockey stick mesogens can respond to the UV irradiation immediately by changing their textures to isotropic liquid and nematic phase reappeared after removing the UV source. This indicated that nematic phase of the bent-core mesogens showed *trans* to *cis* photoisomerization under UV irradiation

and *cis* to *trans* thermal isomerization under visible light irradiation. The azo-functionalised bent-core compounds (**5a-5c**) exhibit the identical photoinduced effect. Of these, the compound (**5c**) is considered as the representative example. The compound **5c** was cooled from the isotropic liquid state to 119.5 °C in the range of the nematic phase (**Fig. 7a**). The sample display nematic phase was exposed to UV irradiation at 366 nm (10 mW/sec²), the schlieren textures of the nematic phase is slowly started disappearing and finally replaced by dark isotropic liquid at 20 s (**Fig 7b**). After removal of the UV lamp, the schlieren texture of the nematic phase reappeared (**Fig.7**). It seems that the *trans*-to-*cis* and *cis*-to-*trans* photoisomerization was observed on the nematic phase of the compounds. Therefore, photoisomerization in a nematic phase of the bent-core mesogens could be useful for light-sensitive displays or data storage applications. It is interesting to note that the absorption maxima for the bent-core compounds (**5a-5c**) fall outside the well-known spectral region of the halogen lamp (~600-950 nm) which is the light source in our POM. The effect of halogen light on the nematic phase of these compounds was studied. The sample slides were observed under the POM which is attached with a hot stage, at varying time intervals under different light conditions. The observations made for the sample (**5c**) are shown in **Fig. 8**. The black texture, (see **Fig. 8a**) is the isotropic phase at a temperature of 119.5 °C and the halogen light was kept dim. Now, we started exposing the sample with a halogen lamp on increasing the intensity of the light, and **Fig. (8b-d)** show the disappearance of the nematic phase as the sample was exposed to light at different time intervals. At this stage, we kept the temperature of the sample constant (117°C) and went on exposing the sample to bright light at different time intervals. **Fig. 8e** show the disappearance of the nematic phase as the sample absorbs more and more light and it goes completely into an isotropic state after 20 s without increasing the temperature. Again, the isotropic dark textures become nematic schlieren texture when the intensity of the halogen light decreases (**Fig. 8f**).

DFT studies

Theoretical calculations (structural relaxation, spectroscopic properties and reactivity parameter) have been done using density functional theory (DFT) method as employed in the Gaussian 09 program package [71]. M06, the hybrid functional [72] and 6-311g basis set [73-74] are employed for the calculation with polarizable continuum solvation model (PCM) and chloroform as a solvent. No geometry constraint has been imposed throughout the calculation. The positive values of vibrational wavenumbers confirm that the optimized molecular structure is stable. The

UV-visible absorption spectra have been simulated using time-dependent density functional theory (TD-DFT). The lowest energy configurations of hockey stick shaped mesogens (both *trans* and *cis* conformation) considering the different position of methyl group are presented in **Fig. 9**. In order to see how electronic property changes with different positions of a methyl group, we have illustrated in **Fig. 10** highest occupied molecular orbital (HOMO) and lowest unoccupied molecular orbital (LUMO) which dictate the stability, reactivity and other properties of the compounds. As the presence of solvent does not introduce any notable change in the position of HOMO and LUMO, we have presented it only for solvent phase. It can be seen from the **Fig. 10** that, both HOMO and LUMO are mainly located on the left arm of the compound irrespective of the position of methyl group and conformation (*cis* or *trans*). The electron density is extending over the entire left arm with contributions from the azo, ester group and methoxybenzene ring. However, HOMO-1 (see ESI **Fig. S6**) is located at core region, imine (-N=CH-) group and phenyl ring of right arm with a negligible contribution from the methoxybenzene of the left arm without depending on the position of a methyl group. Whereas, the core region, -N=C-H group and phenyl ring of the right arm, as well as ester and an azo group of the left arm, contribute to LUMO+1 (see ESI **Fig. S6**) irrespective of the position of the methyl group. Thus, frontier orbitals predict that position of methyl group does not bring any substantial change in its electronic properties.

The molecular electrostatic potential distribution plot of these hockey stick compounds (solvent phase) [**Fig.11**] also support these findings. It is evident that electrostatic molecular electrostatic potential describes the electrostatic potential and charge distribution in a compound which gives the primary idea about the reactive site. Here, the depletion in electronic charge (higher potential), excess in electronic charge (lower potential) and average electrostatic potential are displayed by blue, red and green colour respectively. All oxygen atoms and the nitrogen atom of azo group basically contribute the region with lower electrostatic potential energy due to the presence of negative charge. Out of these lower electrostatic potential regions (higher electronegativity value), the ester group shows the lowest potential in case of *trans* conformation. Whereas for *cis* conformation along with oxygen atoms, the nitrogen atom of the azo group (-N=N-) also exhibits lower potential (higher electronegativity value) among which region near the azo group (-N=N-) has the lowest potential. Hence, these regions with lower potential are the reactive sites and would have a very strong attraction on positively charged

particles. The other region of the compound has average electrostatic potential. The different position of methyl group does not play any vital role on electrostatic potential distribution.

To support the experimental UV-visible absorption spectra, we have compared the theoretically obtained UV-visible absorption spectra (both gaseous and solvent phase) with the experimental one (**Fig. 12**) and the corresponding electronic excitations related to strong peak with highest oscillator strength are listed in **Table 3**. The theoretically obtained strong peak calculated in both gas and solvent phase are red-shifted compared to the experimental one. Theoretically obtained spectra of *trans* conformation contain two peaks for the different position of the methyl group. The first peak appears more or less at the same position as an experimental one but a small shift has been observed for the strong peak. The strong peak of (**5a**) is located at 369.075 nm which is red shifted compared to the experimental one by ~23 nm. However, the substitution of methyl group in the *ortho* position of ester linkage (**5b**) shifted the strong peak at 359.216 nm which is slightly blue shifted compared to compound (**5a**) while substitution of the methyl group in the *meta* position (**5c**) shifted the strong peak at 376.712 nm which is slightly red shifted compared to **5a** compound. The blue/red shift of the absorption peak may be explained by the effect of the electron donating bulky methyl group. The presence of the bulky methyl group at the *ortho* position of the ester linkage (**5b**) increases the twisting angle (~77.721°) as compared to the non-methylated analogue (~56.578°). Therefore, charge conjugation is slightly restricted as a result of which the absorption peak is shifted to shorter wavelength. It is further noted that, the presence of the electron donating methyl group at the *meta* position of the ester group (**5c**) have not greatly change the twisting angle (~59.483 °) but the strong electron donating nature of the methyl group may help in the charge conjugation. Therefore, the absorption peak is shift toward longer wavelength. For both substitution sites, the shift of strong peak is less (~10 for (**5b**); ~7 nm for (**5c**)) with respect to (**5a**) compound and this shift gets reduced for (**5b**) compound due to the inclusion of solvent. To cross-check our result, we have also calculated the UV-visible spectra of *trans* conformation (solvent phase) with higher basis set (6-311+g(d,p)) and found that the substitution by methyl group in *ortho* or *meta* position slightly shifted the strong peak with respect to (**5a**) compound also (see ESI **Figure S7**).

The first peak is mainly characterized by the excitation transitions (HOMO-1) → LUMO, (HOMO-1) → (LUMO+1), whereas the strong peak is mainly originated by the

excitation transitions HOMO \rightarrow LUMO, and (HOMO-1) \rightarrow LUMO. The shape of the spectra for *cis* conformation resembles the experimental one. For *cis* conformation, the spectra contain three peaks. Same as *trans* configuration, the first peak of UV-vis spectra (*cis* conformation) appears at same wavelength irrespective of the substitution site of the methyl group. This peak originates from a lot of weak electronic transitions. The most intense peak of **5a** in the gas phase is found at 329.804 nm with oscillator strength, $f=0.654$ which mainly appears due to the transition between (HOMO-1) \rightarrow (LUMO+1), (HOMO-1) \rightarrow LUMO and (HOMO-4) \rightarrow (LUMO+1). The substitution of the methyl group in *ortho* or *meta* position slightly with respect to ester linkage shifts the strong peak in the gas phase. But in the solvent phase, the strong peak of (**5a**), (**5b**) and (**5c**) compounds are found more or less at the same wavelength as an experimental one. For (**5a**) compound, besides this strong peak, a weak peak is also observed around 555.530 nm in the gas phase (542.193 nm in solvent phase), and this peak arises due to electronic transitions mainly between HOMO \rightarrow LUMO and (HOMO-3) \rightarrow LUMO. The location of this peak changes with methyl substitution site and follow the trend (**5a**) > (**5b**) > (**5c**).

Reactivity parameters are quite successful to describe of reactivity trend and reaction pathway in molecules [75-80]. The excited state phenomena [81-83] and toxicity [84-86] of a molecule can be predicted with the help of these parameters. To shed insight on the chemical reactivity of hockey stick shaped mesogens, we have calculated the ionization potential (*IP*) and electron affinity (*EA*) of these compounds and tabulated in **Table 4**. The *IP* value signifies a tendency of the molecule to remove electrons whereas *EA* value indicates electrons accepting tendency of a compound. With respect to the gas phase, the *IP* value decreases in the solvent phase, while the electron affinity (*EA*) increases. By knowing ionization potential (*IP*) and electron affinity (*EA*) value other chemical reactivity parameters namely chemical potential (μ), chemical hardness (η) and electrophilicity index (ω) can be obtained from the following equation

$$\mu = -\frac{IP+EA}{2} \quad (1)$$

$$\eta = IP - EA \quad (2)$$

$$\omega = \frac{\mu^2}{2\eta} \quad (3)$$

Chemical potential value can be considered as a measurement of electron escaping tendency from the system. We see that chemical potential value is decreased for *cis* conformation than

trans conformation indicating the high electron-attracting power of *cis* conformation. Chemical hardness indicates the stability of a compound. In accordance with the maximum hardness principle (MHP) [87], a chemical system tends to arrange itself to achieve maximum hardness. The larger value of η implies the less reactivity and more stability of a compound. Our calculation (**Table 4**) shows that *trans* conformation has larger chemical hardness than *cis* conformation indicating their greater stability. Moreover, the inclusion of solvent increases the hardness (stability) compared to the gas phase. Thus in presence of the solvent, the compounds become more inert or less reactive. Electrophilicity index measures the tendency of the compound to gain electrons and contains the kinetic and thermodynamic information [88] of the system. It is obvious from **Table 4** that compounds having larger hardness exhibits less electrophilicity *i.e.*, *trans* conformation has low electrophilicity index than *cis* conformation, and hence *cis* conformation is more reactive than *trans* conformation.

The reactivity parameter slightly depends on the substitution site of the methyl group. For both *trans* and *cis* conformation, **5a** compound is most stable. After methyl group substitution, for *trans* conformation, a *meta*-substituted compound is more stable than *ortho* substituted compound, while for *cis* conformation, *ortho* substitute compound is more stable.

Conclusion

We report design and synthesis of new azo functionalised reactive unsymmetrical hockey stick mesogens possessing lateral methyl group. The compounds exhibited a wide range of enantiotropic nematic phase at the ambient temperature. The room temperature nematic phase observed on methyl substitution at the elongated arm of the molecule. Reversible photo-switching behaviour in solution and liquid crystalline state is noted in azo functionalised reactive hockey stick mesogens possessing lateral methyl group. Density functional theory (DFT) calculations show that different position of methyl group does not play any vital role in electronic properties *i.e.* location of HOMO, HOMO-1, LUMO, LUMO+1, electrostatic potential distribution, reactivity profile and spectroscopic properties although a small shift in strong peak is observed in UV-visible absorption spectra due to different position of methyl group. The *trans* conformation has slightly greater stability and less reactivity than *cis* conformation irrespective of methyl group substitution site.

Acknowledgement

This research work was supported by Department of Science and Technology, New Delhi, India (No.SR/S2/CMP-70/2007-I). GK and SKS thanks, University Grants Commission India for University fellowship. Miss Barnali Bhattacharya likes to thanks Council of Scientific and Industrial Research (CSIR), Govt. of India for providing fellowship.

References

- [1] Hafiz HR, Nakanishi F. Photoresponsive liquid crystal display driven by new photochromic azobenzene based Langmuir-Blodgett films. *Nanotechnology* 2003;14:649-654.
- [2] Son JH, Lee SH, Hong SH, Zin WC, Song JK. Photo-controllable electro-optic response of liquid crystalline cells using photo-isomeric molecules. *Liq Cryst* 2013;40:646-655.
- [3] Bobrovsky A, Shibaev V. Polarised light-induced orientation and reorientation processes and unexpected 'memory effect' in side-chain azobenzene containing LC polymers. *Liq Cryst* 2012;39: 339-345.
- [4] Jousseme B, Blanchard P, Gallego-Planas N, Delauney J, Allain M, Richomme P, Levillain E, Roncali J. Largescale synthesis of nearly monodisperse CdSe/CdS core/shell nanocrystals using air-stable reagents via successive ion layer adsorption and reaction. *J Am Chem Soc* 2003;125:2588-2889.
- [5] Mativetsky JM, Pace G, Elbing M, Rampi MA, Mayor M, Samori P. Azobenzenes as light-controlled molecular electronic switches in nanoscale metal-molecule metal junctions. *J Am Chem Soc* 2008;130:9192-9193.
- [6] Mathews M, Zola RS, Yang DK, Li QA. Thermally, photochemically and electrically switchable reflection colors from self-organized chiral bent-core liquid crystals. *J Mater Chem* 2011;21:2098-2103.
- [7] Smaali K, Lenfant S, Karpe S, Ocafrain M, Blanchard P, Deresmes D, Godey S, Rochefort A, Roncali J, Vuillaume D. High on-off conductance switching ratio in optically-driven self-assembled conjugated molecular systems. *ACS Nano* 2010;4:2411-2421.
- [8] Lim LS, Li N, Lu J, Ling Q, Zhu CX, Kang E, Neoh KG. Conductivity switching and electronic memory effect in polymers with pendant azobenzene chromophores. *ACS Appl Mater Inter* 2009;1:60-71.

- [9] Hu JS, Zhang X, Jia YG, Meng QB. Synthesis and phase behaviour of chiral liquid crystalline monomers based on methyl groups, smectic polymers and cholesteric elastomers. *Liq Cryst* 2012;39: 121-131.
- [10] Nunes GE, Sehnem AL, Bechtold IH. Self-assembled azo-dye film as an efficient liquid crystal aligning layer. *Liq Cryst* 2012;39:205-210.
- [11] Natarajan LV, Cazzell SA, Tondiglia VP, Bunning TJ, White TJ. The role of crosslinking and polarity in the dark relaxation of azobenzene-based, polymer-stabilised cholesteric liquid crystals. *Liq Cryst* 2012;39:1450-1457.
- [12] Zettsu N, Ogasawara T, Arakawa R, Nagano S, Ubukata T, Seki T. Highly photosensitive surface relief gratings formation in a liquid crystalline azobenzene polymer: new implications for the migration process. *Macromolecules* 2007;40:4607-4613.
- [13] Nardele CG, Asha SK. Twin liquid crystals and segmented thermotropic polyesters containing azobenzene - effect of spacer length on LC properties. *J Polym Sci Pol Chem* 2012;50:2770-2785.
- [14] Xu Y, Chen X, Zhao F, Fan X, Chen P, An Z. Synthesis and properties of substituted benzoxazole-terminated liquid crystals. *Liq Cryst* 2013;40:197-215.
- [15] Trišovi N, Antanasijevi J, Toth-Katona T, Kohout M, Salamonczyk M, Sprunt S, Jakli A, Fodor-Csorba K. Azo-containing asymmetric bent-core liquid crystals with modulated smectic phases. *RSC Adv* 2015;5:64886-64891.
- [16] Gimeno N, Pintre I, Martínez-Abadía M, Serrano JL, Ros MB. Bentcore liquid crystal phases promoted by azo-containing molecules: from monomers to side chain polymers. *RSC Adv* 2014;4:19694-19702.
- [17] Srinivasan MV, Kannan P, Roy P. Photo and electrically switchable B7 mesophase exhibiting asymmetric bentcore liquid crystals. *New J Chem* 2013;37:1584-1590.
- [18] Nagaveni NG, Roy A, Prasad V. Achiral bent-core azo compounds: effect of different types of linkage groups and their direction of linking on liquid crystalline properties. *J Mater Chem* 2012;22:8948-8959.
- [19] Rahman L, Kumar S, Tschierske C, Israel G, Ster D, Hegde G. Synthesis and photoswitching properties of bent-shaped liquid crystals containing azobenzene monomers. *Liq Cryst*. 2009;36:397-407.

- [20] Alaasar M. Azobenzene-containing bent-core liquid crystals: an overview. *Liq Cryst* 2016;43:2208-2243.
- [21] Saha SK, Paul MK. Mesomorphic and photophysical behaviour of 1,3,4-oxadiazole based hockey stick reactive mesogens, *Liq Cryst*. 2018; DOI: 10.1080/02678292.2018.1502372
- [22] Espinosa MA, Cadiz V, Galia M. New cholesteric liquid-crystal epoxy resins derived from 6-hydroxy- 2-naphthoic acid. *J Poly Sci Pol Chem* 2001;39: 2847-2858.
- [23] Hu JS, Zhang BY, Sun K, Li QY. Side chain cholesteric liquid crystalline elastomers: synthesis and phase behaviour. *Liq Cryst* 2003;30:1267–1275.
- [24] Zhang BY, Hu JS, Jia YG, Du BG. Side-chain cholesteric liquid crystalline elastomers derived from nematic *bis*-olefinic crosslinking units. *Macromol Chem Phys* 2003;204:2123-2129.
- [25] Thomsen DL, Keller P, Naciri J, Pink R, Jeon H, Shenoy D, Ratna BR. Liquid crystal elastomers with mechanical properties of a muscle. *Macromolecules* 2001; 34:5868-5875.
- [26] Garcia-Amorós J, Velasco D. (2015) Azobenzene-Containing Liquid Single Crystal Elastomers for Photoresponsive Artificial Muscles. In: Thakur V., Kessler M. (eds) *Liquid Crystalline Polymers*. Springer, Cham.
- [27] Iqbal D, Samiullah MH. Photo-responsive shape memory and shape-changing liquid-crystal polymer networks. *Materials* 2013;6:116-142.
- [28] Cook AG, Inkster RT, Martinez-Felipe A, Ribes- Greus A, Hamley IW, Imrie CT. Synthesis and phase behaviour of a homologous series of polymethacrylatebased side-chain liquid crystal polymers. *Eur Polym J* 2012;48:821-829.
- [29] Gutiérrez-Cuevas KG, Larios-López L, Rodríguez- González RJ, Donnio B, Navarro-Rodríguez D. On the liquid-crystalline properties of methacrylic polymers containing 4-(4-alkyloxyphenyl) azobenzene mesogens. *Liq Cryst* 2013;40:534-545.
- [30] Niori T, Sekine T, Watanabe J, Furukawa T, Takezoe H. Distinct ferroelectric smectic liquid crystals consisting of banana shaped achiral molecules. *J Mater Chem* 1996, **6**, 1231-1233.
- [31] Link DR, Natale G, Shao R, MacLennan EJ, Clark NA, Korblova E, Walba DM. Spontaneous formation of macroscopic chiral domains in a fluid smectic phase of achiral molecules. *Science* 1997;278:1924-1927.
- [32] Pelzl G, Diele S, Weissflog W. Banana-Shaped Compounds-A New Field of Liquid Crystals. *Adv Mater* 1999;11:707-724.

- [33] Reddy RA, Tschierske C. Bent-core liquid crystals: polar order, superstructural chirality and spontaneous desymmetrisation in soft matter systems. *J Mater Chem* 2006;16: 907-961.
- [34] Ros MB, Serrano JL, de la Fuente MR, Folcia CL. Banana-shaped liquid crystals: a new field to explore. *J Mater Chem* 2005;15:5093-5098.
- [35] Takezoe H, Takanishi Y. Bent-Core Liquid Crystals: Their Mysterious and Attractive World. *Jpn J Appl Phys* 2006;45:597-625.
- [36] Harden J, Mbanga B, Eber N, Fodor-Csorba K, Sprunt S, Gleeson JT, Jakli A. Giant Flexoelectricity of Bent-Core Nematic Liquid Crystals. *Phys Rev Lett* 2006;97:157802.
- [37] Shanker G, Nagaraj M, Kocot A, Vij JK, Prehm M, Tschierske C. Nematic phases in 1,2,4-Oxadiazole-based bent-core liquid crystals: is there a ferroelectric switching? *Adv Funct Mater* 2012;22:1671-1683.
- [38] Wiant DB, Gleeson JT, Eber N, Fodor-Csorba K, Jakli A, Toth-Katona T. Nonstandard electroconvection in a bent-core nematic liquid crystal. *Phys Rev E* 2005;72: 041712.
- [39] Wiant D, Stojadinovic S, Neupane K, Sharma S, Fodor-Csorba K, Jakli A, Gleeson JT, Sprunt S. Critical behavior at the isotropic-to-nematic phase transition in a bent-core liquid crystal. *Phys Rev E* 2006;73(R): 030703.
- [40] Ghosh S, Begum N, Turlapati S, Roy SK, Das AK, Rao NVS. Ferroelectric-like switching in the nematic phase of four-ring bent-core liquid crystals. *J Mater Chem C* 2014;2: 425-431.
- [41] Keith C, Lehmann A, Baumeister U, Prehm M, Tschierske C. Nematic phases of bent-core mesogens. *Soft Matter* 2010;6:1704-1721.
- [42] Francescangeli O, Stanic V, Torgova SI, Strigazzi A, Scaramuzza N, Ferrero C, Dolbnya IP, Weiss TM, Berardi R, Muccioli L, Orlandi S, Zannoni C. Ferroelectric Response and Induced Biaxiality in the Nematic Phase of Bent-Core Mesogens. *Adv Funct Mater* 2009;19:2592-2600.
- [43] Francescangeli O, Samulski ET. Insights into the cybotactic nematic phase of bent-core molecules. *Soft Matter* 2010;6:2413-2420.
- [44] Chakraborty S, Gleeson JT, Jakli A, Sprunt S. A comparison of short-range molecular order in bent-core and rod-like nematic liquid crystals. *Soft Matter* 2013;9:1817-1824.
- [45] Zhang C, Gao M, Diorio N, Weissflog W, Baumeister U, Sprunt S, Gleeson JT, Jakli A. Direct Observation of Smectic Layers in Thermotropic Liquid Crystals. *Phys Rev Lett* 2012;109: 107802.

- [46] Chen D, Nakata M, Shao R, Tuchband MR, Shuai M, Baumeister U, Weissflog W, Walba DM, Glaser MA, MacLennan JE, Clark NA. Twist-bend heliconical chiral nematic liquid crystal phase of an achiral rigid bent-core mesogen. *Phys Rev E* 2014;89:022506.
- [47] Archarya BR, Primak A, Dingemans TJ, Primak A, Dingemans TJ, Samulski ET, Kumar S. The elusive thermotropic biaxial nematic phase in rigid bent-core molecules. *Pramana-J Phys* 2003;61:231-237.
- [48] Acharya BR, Primak A, Kumar S. Biaxial nematic phase in bent-core thermotropic mesogens. *Phy Rev Lett* 2004;92:145506.
- [49] Deb R, Nath RK, Paul MK, Rao NVS, Tuluri F, Shen Y, Shao R, Chen D, Zhu C, Smalyukh II, Clark NA. Four-ring achiral unsymmetrical bent core molecules forming strongly fluorescent smectic liquid crystals with spontaneous polar and chiral ordered B7 and B1 phases. *J Mater Chem* 2010;20:7332-7336.
- [50] Paul MK, Nath RK, Moths B, Pan LD, Wang S, Deb R, Shen Y, Rao NVS, Huang CC. Layer thinning transition in an achiral four-ring hockey stick shaped liquid crystal. *Phase Transitions* 2012;85:1070-1078.
- [51] Saha SK, Paul MK, Chandran A, Khanna PK, Biradar AM. Low-temperature nematic phase in asymmetrical 1,3,4-oxadiazole bent core liquid crystals possessing lateral methoxy group *Liq. Cryst.*, 2017; 44:1739-1750.
- [52] Nafees A, Kalita G, Paul MK, Sinha A, Rao NVS. Effect of methoxy group instead of polar group in the nematic phase of four-ring bent-core liquid crystals. *RSC Adv* 2015;5:7001-7006.
- [53] Alaasar M, Poppe S, Tschierske C. Cybotactic nematic phases of photoisomerisable hockey-stick liquid crystals, *Liq Cryst* 2017; 44:729-737.
- [54] Paul MK, Kalita G, Laskar AR, Debnath S, Gude V, Sarkar DD, Mohiuddin G, Varshney SK, Rao NVS. Synthesis and mesomorphic behaviour of achiral four-ring unsymmetrical bent-core liquid crystals: Nematic phases. *J Mol Struct* 2013, 1049, 78-89.
- [55] Upadhyaya K, Gude V, Mohiuddin G, Rao NVS. A new family of four rings bent-core nematic liquid crystals with highly polar transverse and end groups. *Beilstein J Org Chem* 2013;9:26-35.
- [56] Sarkar DD, Deb R, Chakraborty N, Rao NVS. Synthesis of achiral four-ring unsymmetrically substituted toluene derived liquid crystals with a polar end group. *Liq Cryst* 2012;39:1003-1010.

- [57] Gude V, Upadhyaya K, Mohiuddin G, Rao NVS. A new family of four-ring bent-core nematic liquid crystals with a highly polar end-group. *Liquid Crystals* 2013;40:120-129.
- [58] Debnath S, Mohiuddin G, Turlapati S, Begum N, Sarkar DD, Rao NVS. Nematic phases in achiral unsymmetrical four-ring bent-core azo compounds possessing strongly polar cyano and nitro moieties as end substituents: Synthesis and characterization. *Dyes Pigm* 2013;99:447-445.
- [59] Nafees A, Sinha A, Rao NVS, Kalita G, Mohiuddin G, Paul MK. Design, synthesis and mesomorphic behaviour of a four-ring achiral bent-core liquid crystal in the nematic phase. *RSC Adv* 2016;6:43069-43079.
- [60] Stewart D, Imrie CT. Synthesis and characterization of spin-labelled and spin-probed side-chain liquid crystal polymers. *Polymer* 1996;37:3419-3425.
- [61] Hillemann CL, Van Hecke GR, Peak SR, Winther JB, Rudat MA, Kalman DA, White ML. Physical studies of homologous trans-4-ethoxy-4'-n-Alkanoyl oxyazobenzenes. *J Phys Chem* 1975; 79:1566-1571.
- [62] Wang G, Zhang M, Zhang T, Guan J, Yang H. Photoresponsive behaviors of smectic liquid crystals tuned by an azobenzene chromophore. *RSC Adv* 2012; 2:487-493.
- [63] Lai CK, Chang CH, Tsai CH. Liquid crystalline properties of bis(salicylaldiminato)copper(II) complexes: the first columnar discotics derived from salicylaldimine Schiff bases. *J Mater Chem* 1998;8:599-602.
- [64] Binnemans K, Galyametdinov YG, Collinsonc SR, Bruce DW. Reduction of the transition temperatures in mesomorphic lanthanide complexes by the exchange of counter-ions. *J Mater Chem* 1998;8:1551-1553.
- [65] Pintre IC, Gimeno N, Serrano JL, Ros MB, Alonso I, Folcia CL, Ortega J, Etxebarria J. Liquid crystalline and nonlinear optical properties of bent-shaped compounds derived from 3,4'-biphenylene. *J Mater Chem* 2007;17:2219-2227.
- [66] Kim Y-K, Cukrov G, Xiang J, Shin S-T, Lavrentovich OD. Domain walls and anchoring transitions mimicking nematic biaxiality in the oxadiazole bent-core liquid crystal C7. *Soft Matter* 2015;11:396-3970.
- [67] Vaupotiċ N, Szydłowska J, Salamonczyk M, Kovarova A, Svoboda J, Osipov M, Pocięcha D, Gorecka E. Structure studies of the nematic phase formed by bent-core molecules. *Phys Rev E* 2009;80: 030701(R).

- [68] Singh S, Deb R, Chakraborty N, Singh H, Gupta V, Sinha K, Tandon P, Omelchenko M, Rao N V S , Ayala AP. A combined experimental and theoretical approach to study $\text{SmC} \rightarrow \text{N}_{\text{cybC}}$ phase transition in a four-ring bent-core liquid crystal. *New J Chem* 2016;40: 6834-6847.
- [69] Chakraborty L, Chakraborty N, Sarkar DD, Rao NVS, Aya S, Le KV, Araoka F, Ishikawa K, Pocięcha D, Gorecka E, Takezoe H. Unusual temperature dependence of smectic layer structure associated with the nematic-smectic C phase transition in a hockey-stick-shaped four-ring compound. *J Mater Chem C* 2013;1:1562–1566.
- [70] Lehmann M, Seltmann J. Low temperature enantiotropic nematic phases from V-shaped, shape-persistent molecules. *J. Beilstein J. Org. Chem.* 2009; 73.doi:10.3762/bjoc.5.73.
- [71] M.J. Frisch, G.W. Trucks, H.B. Schlegel, G.E. Scuseria, M.A. Robb, J.R. Cheeseman, G. Scalmani, V. Barone, B. Mennucci, G.A. Petersson, H. Nakatsuji, M. Caricato, X. Li, H.P. Hratchian, A.F. Izmaylov, J. Bloino, G. Zheng, J.L. Sonnenberg, M. Hada, M. Ehara, K. Toyota, R. Fukuda, J. Hasegawa, M. Ishida, T. Nakajima, Y. Honda, O. Kitao, H. Nakai, T. Vreven, J.A. Montgomery Jr., J.E. Peralta, F. Ogliaro, M. Bearpark, J.J. Heyd, E. Brothers, K.N. Kudin, V.N. Staroverov, T. Keith, R. Kobayashi, J. Normand, K. Raghavachari, A. Rendell, J.C. Burant, S.S. Iyengar, J. Tomasi, M. Cossi, N. Rega, J.M. Millam, M. Klene, J.E. Knox, J.B. Cross, V. Bakken, C. Adamo, J. Jaramillo, R. Gomperts, R.E. Stratmann, O. Yazyev, A.J. Austin, R. Cammi, C. Pomelli, J.W. Ochters, R.L. Martin, K. Morokuma, V.G. Zakrzewski, G.A. Voth, P. Salvador, J.J. Dannenberg, S. Dapprich, A.D. Daniels, O. Farkas, J.B. Foresman, J.V. Ortiz, J. Cioslowski, D.J. Fox, Gaussian 09, Revision B.01, Gaussian Inc., Wallingford CT, 2010.
- [72] Zhao Y, Truhlar DG. The M06 suite of density functionals for main group thermochemistry, thermochemical kinetics, noncovalent interactions, excited states, and transition elements: two new functionals and systematic testing of four M06-class functionals and 12 other functionals, *Theor Chem Acc* 2008; 120:215-241.
- [73] McLean AD, Chandler GS. Contracted Gaussian-basis sets for molecular calculations. 1. 2nd row atoms, Z=11-18. *J Chem Phys* 1980; 72: 5639-5648.
- [74] Curtiss LA, McGrath MP, Blaudeau J-P, Davis NE, Binning Jr. RC, Radom L. Extension of Gaussian-2 theory to molecules containing third-row atoms Ga-Kr. *J Chem Phys* 1995; 103: 6104-6113.

- [75] Chattaraj PK, Sarkar U. Effect of spherical confinement on chemical reactivity. *J Phys Chem A* 2003;107:4877-4882.
- [76] Chattaraj PK, Maiti B, Sarkar U. Chemical reactivity of the compressed noble gas atoms and their reactivity dynamics during collisions with protons. *J Chem Sci* 2003;115:195-218.
- [77] Chattaraj PK, Khatua M, Sarkar U. Reactivity Dynamics of a Confined Molecule in Presence of an External Magnetic Field. *Int J Quantum Chem* 2015; 115:144-157.
- [78] Khatua M, Sarkar U, Chattaraj PK. Reactivity dynamics of confined atoms in the presence of an external magnetic field. *Eur Phys J D* 2014;68:22.
- [79] Chattaraj PK, Maiti B, Sarkar U. Philicity: a unified treatment of chemical reactivity and selectivity. *J Phys Chem A* 2003;107:4973-4975.
- [80] Chattaraj PK, Sarkar U, Parthasarathi R, Subramanian V. DFT study of some aliphatic amines using generalized philicity concept. *Int J Quantum Chem* 2005;101:690-702.
- [81] Chattaraj PK, Sarkar U. Ground-and excited-states reactivity dynamics of hydrogen and helium atoms. *Int J Quantum. Chem* 2003; 91:633-650.
- [82] Sarkar U, Khatua M, Chattaraj PK. A tug-of-war between electronic excitation and confinement in a dynamical context, *Phys Chem Chem Phys* 2012;14:1716-1727.
- [83] Chattaraj PK, Sarkar U. Chemical reactivity dynamics in ground and excited electronic states. *Comput. Theor. Chem* 2007; 19:269-286.
- [84] Elango M, Parthasarathi R, Subramanian V, Sarkar U, Chattaraj PK. Formaldehyde decomposition through profiles of global reactivity indices. *J Mol Struct THEOCHEM* 2005; 723:43-52
- [85] Parthasarathi R, Padmanabhan J, Subramanian V, Sarkar U, Maiti B, Chattaraj PK. Toxicity analysis of benzidine through chemical reactivity and selectivity profiles: a DFT approach. *IEJMD* 2003; 2:798-813.
- [86] Sarkar U, Roy DR, Chattaraj PK, Parthasarathi R, Padmanabhan J, Subramanian V. A conceptual DFT approach towards analysing toxicity. *J Chem Sci* 2005;117:599-612.

[87] Pan S, Solà M, Chattaraj PK. On the validity of the maximum hardness principle and the minimum electrophilicity principle during chemical reactions. *J. Phys. Chem. A* 2013; 117:1843-1852.

[88] Chattaraj PK, Sarkar U, Roy DR, Elango M, Parthasarathi R, Subramanian V. Is electrophilicity a kinetic or a thermodynamic concept? *Indian J Chem* 2006;45A:1099-1112.

List of Tables

Table 1. Phase transition temperatures ($^{\circ}\text{C}$) and nematic phase thermal range of the compounds recorded at $5\text{ }^{\circ}\text{C min}^{-1}$ from differential scanning calorimetry (DSC) and confirmed by polarised optical microscopy (POM). The enthalpies (ΔH in kJmol^{-1}) and entropies (ΔS in $\text{Jmol}^{-1}\text{K}^{-1}$), respectively, are presented in parentheses. $\Delta T_{\text{N}} = T_{\text{N-I}} - T_{\text{Cr-N}}$, is in cooling cycle, where $T_{\text{N-I}}$ is nematic-isotropic transition temperature and $T_{\text{Cr-N}}$ is crystal-nematic transition temperatures.

Table 2. UV-visible absorption of compounds (**5a-5c**) in chloroform solvent at $c = 1 \times 10^{-5}\text{M}$.

Table 3. Calculated electronic transitions for maximum peak in UV-visible absorption spectra in of hockey stick mesogens (**5a-5c**) in gas medium and solvent phase.

Table 4. Calculated values of chemical potential (μ), chemical hardness (η) and electrophilicity index (ω) of hockey stick shaped mesogens (**5a-5c**) in gas medium and solvent.

Table 1. Phase transition temperatures ($^{\circ}\text{C}$) and nematic phase thermal range of the compounds recorded at $5\text{ }^{\circ}\text{C min}^{-1}$ from differential scanning calorimetry (DSC) and confirmed by polarised optical microscopy (POM). The enthalpies (ΔH in kJmol^{-1}) and entropies (ΔS in $\text{Jmol}^{-1}\text{K}^{-1}$), respectively, are presented in parentheses. $\Delta T_{\text{N}} = T_{\text{N-I}} - T_{\text{Cr-N}}$, is in cooling cycle, where $T_{\text{N-I}}$ is nematic-isotropic transition temperature and $T_{\text{Cr-N}}$ is crystal-nematic transition temperatures.

Compound	X	Y	Phase Transitions in $^{\circ}\text{C}$ (enthalpy and entropy)	ΔT_{N} ($^{\circ}\text{C}$)
5a	H	H	Cr 122.4 (41.88, 105.7) N 161.0(0.33, 0.76) Iso	38.6
			Cr 78.4(22.74, 102.07) N 158.8(0.27, 0.63) Iso	80.4
5b	CH_3	H	Cr 117.4 (42.69, 109.34) N 128.2 (0.14, 0.35) Iso	10.8
			Iso 126.9 (0.36, 1.39) N 54.9 [†] Cr	72
5c	H	CH_3	Cr 99.4 (45.9, 123.3) N 120.0 (0.3, 0.8) Iso	20.6
			Iso 118.1(0.4, 0.9) N r.t.	88.1

[†] indicated obtained by polarizing optical microscope.

Table 2. UV-visible absorption of compounds (**5a-5c**) in chloroform solvent at $c = 1 \times 10^{-5}\text{M}$

Compound	Conditions	Absorption ($\lambda_{\text{max}}/\text{nm}$)	Molar extinction coefficient ($\epsilon/\text{Lmol}^{-1}\text{cm}^{-1}$)	Assignment
5a	Virgin sample	346	28711	$\pi-\pi^*$
		438	1443	$n-\pi^*$
	Exposed with 366 nm light for 30min	332 438	20896 2177	$\pi-\pi^*$ $n-\pi^*$
5b	Virgin sample	346	27038	$\pi-\pi^*$
		438	1574	$n-\pi^*$
	Exposed with 366 nm light for 30min	334 441	20681 1965	$\pi-\pi^*$ $n-\pi^*$
5c	Virgin sample	346	27349	$\pi-\pi^*$
		438	1346	$n-\pi^*$
	Exposed with 366 nm light for 30min	332 438	22612 3020	$\pi-\pi^*$ $n-\pi^*$
5c	After keeping 24 h in dark	346	26102	$\pi-\pi^*$
		338	1346	$n-\pi^*$

Table 3. Calculated electronic transitions for maximum peak in UV-visible absorption spectra of hockey stick mesogens (**5a-5c**) in gas medium and solvent phase.

Medium	Compound	Maximum peak at wavelength (λ_{max})	Highest oscillator strength (f)	Transitions
Trans (peak A)				
Gas phase	5a	283.682	0.126	HOMO-4 \rightarrow LUMO (15%), HOMO-4 \rightarrow LUMO+1 (24%), HOMO-1 \rightarrow LUMO+2 (10%), HOMO \rightarrow LUMO+2 (21%)
	5b	282.435	0.224	HOMO-4 \rightarrow LUMO+1 (30%), HOMO-3 \rightarrow LUMO (41%) HOMO-11 \rightarrow LUMO+1 (2%)
	5c	282.893	0.223	HOMO-4 \rightarrow LUMO (22%), HOMO-4 \rightarrow LUMO+1 (36%), HOMO-3 \rightarrow LUMO+1 (11%)
Solvent phase	5a	285.045	0.256	HOMO-4 \rightarrow LUMO (19%), HOMO-4 \rightarrow LUMO+1 (42%), HOMO-3 \rightarrow LUMO+1 (14%)
	5b	283.196	0.347	HOMO-4 \rightarrow LUMO+1 (51%), HOMO-3 \rightarrow LUMO+1 (16%) HOMO-11 \rightarrow LUMO+1 (2%)
	5c	284.751	0.214	HOMO-4 \rightarrow LUMO (12%), HOMO-4 \rightarrow LUMO+1 (31%), HOMO-3 \rightarrow LUMO+1 (11%)
Trans (peak B)				
Gas phase	5a	369.075	1.587	HOMO \rightarrow LUMO (96%)
	5b	359.216	1.396	HOMO \rightarrow LUMO (95%)
	5c	376.712	1.450	HOMO \rightarrow LUMO (93%) HOMO-1 \rightarrow LUMO (4%)
Solvent phase	5a	379.978	1.409	HOMO \rightarrow LUMO (94%) HOMO-1 \rightarrow LUMO (4%)
	5b	376.346	1.348	HOMO \rightarrow LUMO (97%)
	5c	388.358	1.325	HOMO \rightarrow LUMO (97%)
Cis (peak B)				
Gas phase	5a	329.804	0.654	HOMO-1 \rightarrow LUMO+1 (73%) HOMO-4 \rightarrow LUMO+1 (7%), HOMO-1 \rightarrow LUMO (8%),
	5b	332.003	0.664	HOMO-1 \rightarrow LUMO (10%), HOMO-1 \rightarrow LUMO+1 (73%) HOMO-4 \rightarrow LUMO+1 (5%)
	5c	330.349	0.639	HOMO-1 \rightarrow LUMO+1 (79%) HOMO-4 \rightarrow LUMO+1 (8%), HOMO-1 \rightarrow LUMO (4%),
Solvent phase	5a	335.190	0.725	HOMO-1 \rightarrow LUMO+1 (69%)

				HOMO-4→LUMO+1 (5%), HOMO-3→LUMO (7%),
	5b	334.746	0.761	HOMO-1→LUMO+1 (79%) HOMO-4→LUMO+1 (6%), HOMO-3→LUMO (3%)
	5c	334.214	0.795	HOMO-1→LUMO+1 (83%) HOMO-4→LUMO+1 (6%),
Cis (peak C)				
Gas phase	5a	555.530	0.040	HOMO→LUMO (85%) HOMO-3→LUMO (5%) HOMO→LUMO+1 (4%)
	5b	552.584	0.035	HOMO→LUMO (82%) HOMO-2→LUMO (6%), HOMO→LUMO+1 (8%)
	5c	544.838	0.030	HOMO→LUMO (88%) HOMO-2→LUMO (5%)
Solvent phase	5a	542.193	0.051	HOMO→LUMO (86%) HOMO-3→LUMO (8%)
	5b	541.365	0.0477	HOMO→LUMO (87%) HOMO-3→LUMO (9%)
	5c	536.260	0.0421	HOMO→LUMO (88%) HOMO-3→LUMO (7%)

Table 4. Calculated values of chemical potential (μ), chemical hardness (η) and electrophilicity index (ω) of hockey stick mesogens (**5a-5c**) in gas medium and solvent.

Medium	Compound	IP (eV)	EA (eV)	μ (eV)	η (eV)	Ω (eV)
Trans						
Gas	5a	7.204	-1.281	-2.962	8.485	0.517
	5b	7.227	-1.189	-3.019	8.416	0.542
	5c	7.167	-1.276	-2.946	8.443	0.514
Solvent	5a	6.503	-2.462	-2.021	8.965	0.228
	5b	6.508	-2.421	-2.044	8.929	0.234
	5c	6.463	-2.468	-1.998	8.931	0.223
Cis						
Gas	5a	7.144	-1.102	-3.021	8.247	0.553
	5b	7.124	-1.078	-3.023	8.202	0.557
	5c	7.140	-1.057	-3.041	8.198	0.564

Solvent	5a	6.339	-2.213	-2.063	8.552	0.249
	5b	6.314	-2.168	-2.073	8.482	0.253
	5c	6.328	-2.151	-2.089	8.479	0.257

List of Figures

Scheme1. Synthetic details of the hockey stick compounds. Reagent and conditions: (i) Dry acetone, KHCO_3 , $\text{CH}_2=\text{CH}(\text{CH}_2)_9\text{Br}$, KI; (ii) 5% Pd/C, H_2 , dry EtOAc, stirring 48 h; (iii) Abs. EtOH, 2-3 drops of glacial acetic acid, reflux 6h; (iv) HCl, NaNO_2 , 0-5 °C, phenol or *o*-cresol or *m*-cresol, NaOH; (v) DCC, DMAP, DCM, stirring 48 h.

Fig 1. DSC thermogram of compound **5a** at scan rate of 5°Cmin⁻¹.

Fig 2. Polarising optical microscopic texture of the compound (**5a**). (a) two brush defect texture of N phase at 173 °C. (b) Co-existence of N-Cr transition at 83.2 °C.

UV-Visible spectra of compounds in chloroform ($c= 1 \times 10^{-5}\text{M}$).

Fig. 3. Fig.3. DSC thermogram of the compound (**5b**) at heating and cooling rate of 5 °Cmin⁻¹.

Fig 4. Polarising optical microscopic textures of the compound (**5b**). (a) Growth of the schlieren texture from isotropic liquid at 127.7 °C; (b) homeotropic texture at 127.6 °C; (c) appearance of thread like texture from homeotropic region at 127.5 °C; (d) thread texture of the nematic phase at 127.4 °C; (e) Co-existence of N-Cr transition at 53.8 °C.

Fig. 5. UV-visible absorption spectra of compounds (**5a-5c**) in chloroform ($c= 1 \times 10^{-5}\text{M}$). Inset represents the expanded region of 400-500 nm.

Fig. 6. UV-visible absorption spectra of **5c** in chloroform ($c= 1 \times 10^{-5}\text{M}$). (a) Freshly prepared sample of *trans*-isomer before irradiation. (b) *Cis* isomer obtained after irradiation with UV-light (366 nm) for 30 min. (c) Irradiated solution after keeping in dark for 24 h. Inset represents the expanded region of 400-500 nm.

Fig 7. Change in the optical texture of the nematic phase on irradiation of the UV light (366 nm) at 119 °C in different time interval. (a) 0 sec; (b) 20 sec.

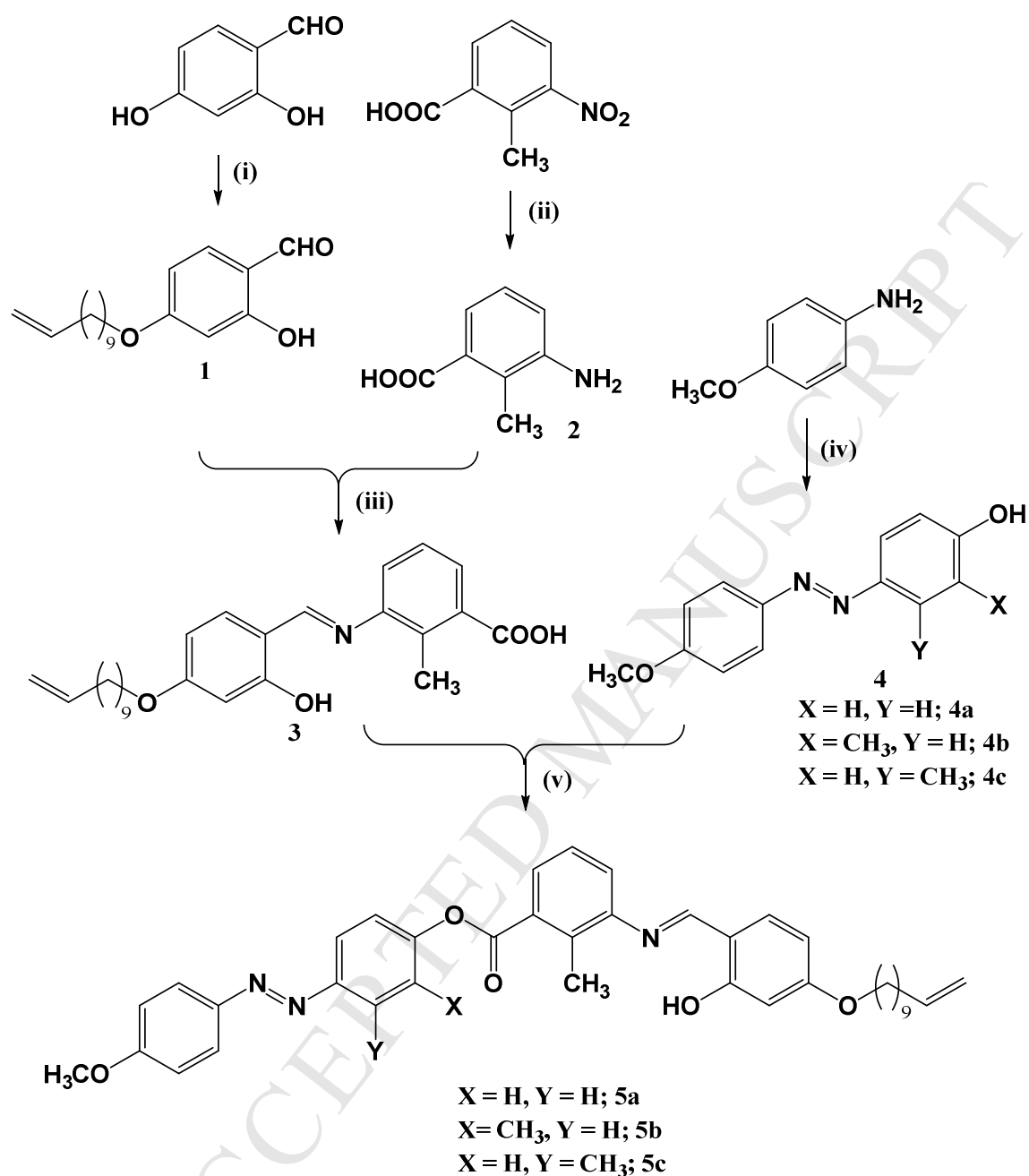
Fig 8. POM textures of the compound **5c** at constant temperature 119.5 °C on increasing the intensity of the halogen lamp light in a nematic phase: (a) Nematic phase; (b), (c) and (d) show isotropic region increase on increasing the intensity of the light; (e) isotropic liquid; (e) appearance of the schlieren texture of nematic phase.

Fig. 9. Optimized geometry of hockey stick shaped mesogens compounds considering different positions of methyl group with respect to azo and /or ester group; (i) *trans* conformation (ii) *cis* conformation. (a) **5a**; (b) **5b**; (c) **5c**.

Fig. 10. Location of highest occupied molecular orbital (HOMO), lowest unoccupied molecular orbital (LUMO) of compounds (**5a-5c**) in solvent phase (a) **5a**; (b) **5b**; (c) **5c**.

Fig. 11. The molecular electrostatic potential distribution of compounds (**5a-5c**) in solvent phase for both *trans* and *cis* conformations.

Fig. 12. UV-visible absorption spectra of compound (**5a-5c**) in (a) gas phase (b) solvent phase. Here (i) and (ii) represents the *trans* conformation and *cis* conformation respectively.



Scheme 1. Synthetic details of the hockey stick compounds. Reagents and conditions: (i) Dry acetone, $KHCO_3$, $CH_2=CH(CH_2)_9Br$, KI, reflux, 48 h.; (ii) 5% Pd/C, H_2 , dry Ethyl acetate, stirring 48 h.; (iii) Absolute EtOH, 2-3 drops of glacial acetic acid, reflux 6h.; (iv) HCl, $NaNO_2$, 0-5 °C, phenol or *o*-cresol or *m*-cresol, NaOH; (v) DCC, DMAP, DCM, stirring 48 h.

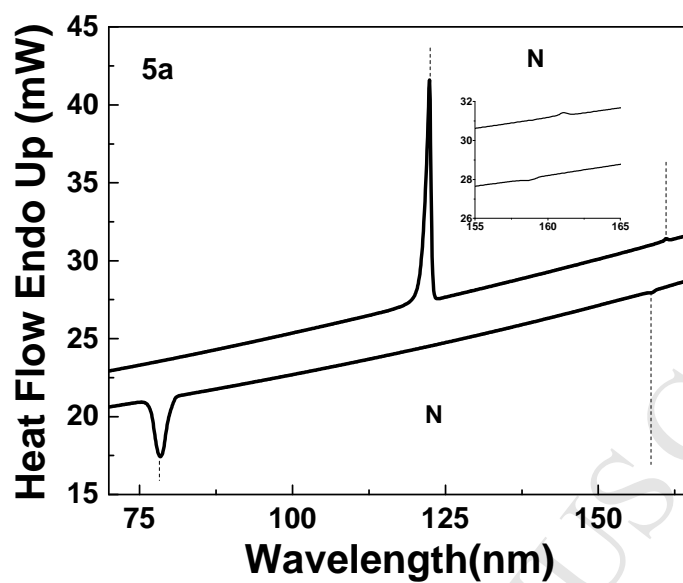


Fig.1. DSC thermogram of compound **5a** at scan rate of $5\text{ }^{\circ}\text{Cmin}^{-1}$.

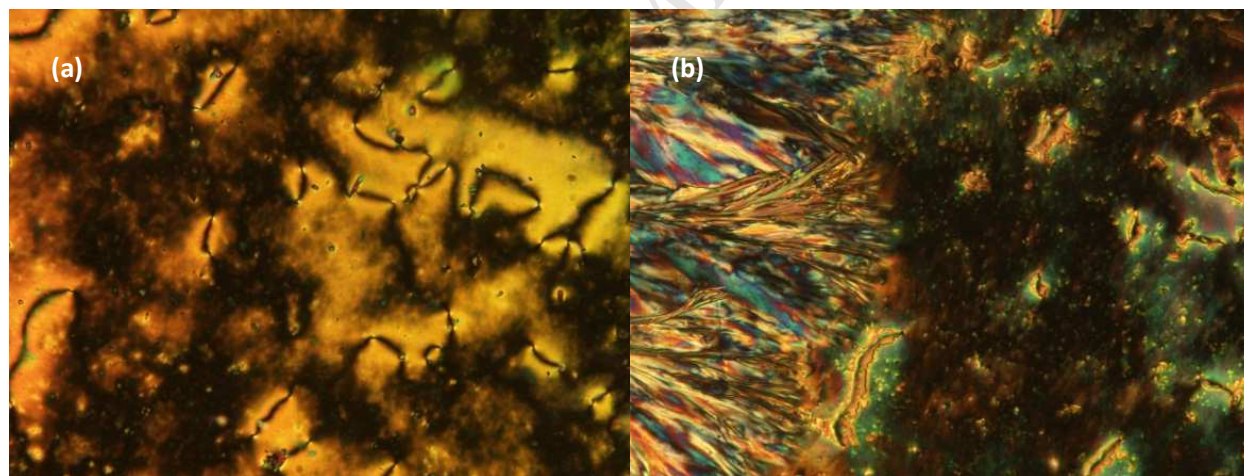


Fig 2. Polarising optical microscopic texture of the compound (**5a**). (a) two brush defect texture of N phase at $158.8\text{ }^{\circ}\text{C}$. (b) Co-existence of N-Cr transition at $78.4\text{ }^{\circ}\text{C}$.

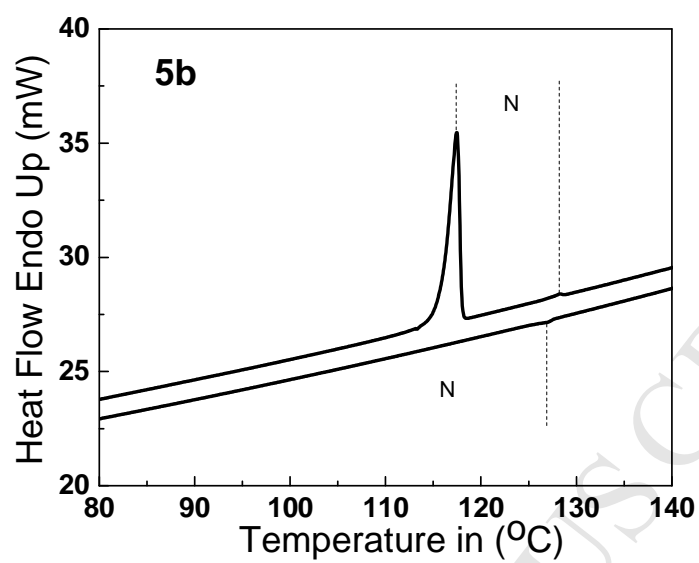


Fig.3. DSC thermogram of the compound (**5b**) at heating and cooling rate of $5\text{ }^{\circ}\text{Cmin}^{-1}$.

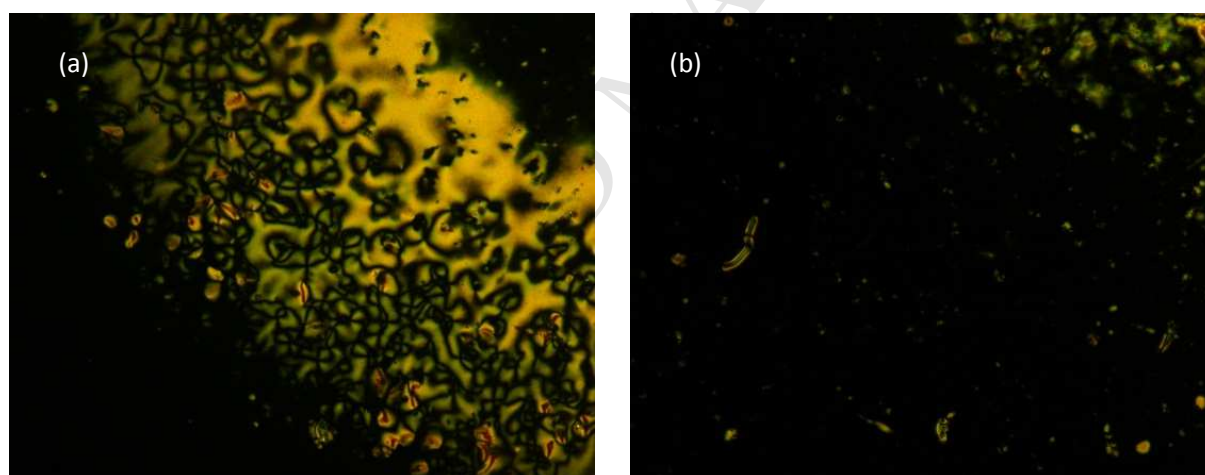




Fig 4. Polarising optical microscopic textures of the compound (**5b**). (a) Growth of the schlieren texture from isotropic liquid at 127.7 °C; (b) homeotropic texture at 127.6 °C; (c) appearance of thread like texture from homeotropic region at 127.5 °C; (d) thread texture of the nematic phase at 127.4 °C; (e) Co-existence of N-Cr transition at 54.9 °C.

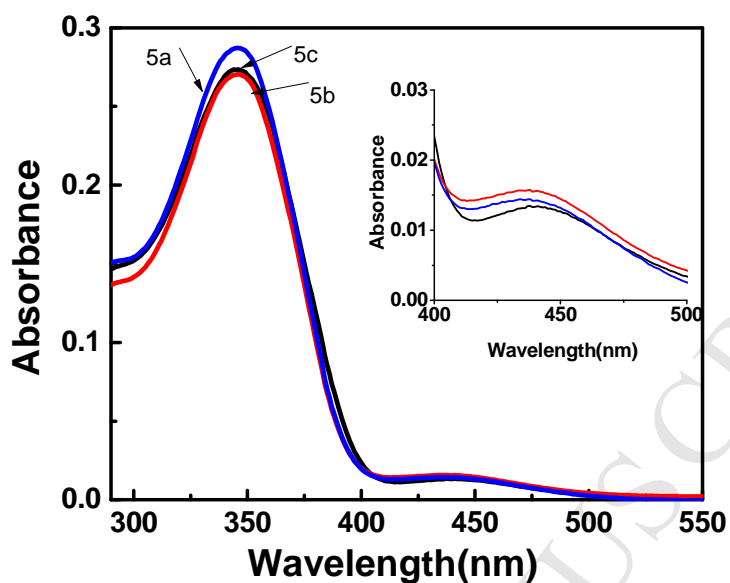


Fig. 5. UV-visible absorption spectra of compounds (**5a-5c**) in chloroform ($c= 1 \times 10^{-5} \text{M}$). Inset represents the expanded region of 400-500 nm.

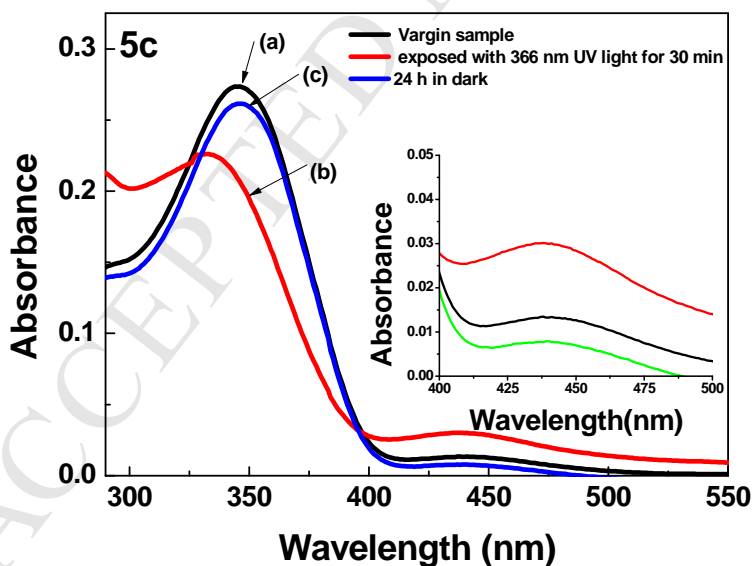


Fig. 6. UV-visible absorption spectra of **5c** in chloroform ($c= 1 \times 10^{-5} \text{M}$). (a) Freshly prepared sample of *trans*-isomer before irradiation. (b) *Cis* isomer obtained after irradiation with UV-light (366 nm) for 30 min. (c) Irradiated solution after keeping in dark for 24 h. Inset represents the expanded region of 400-500 nm.

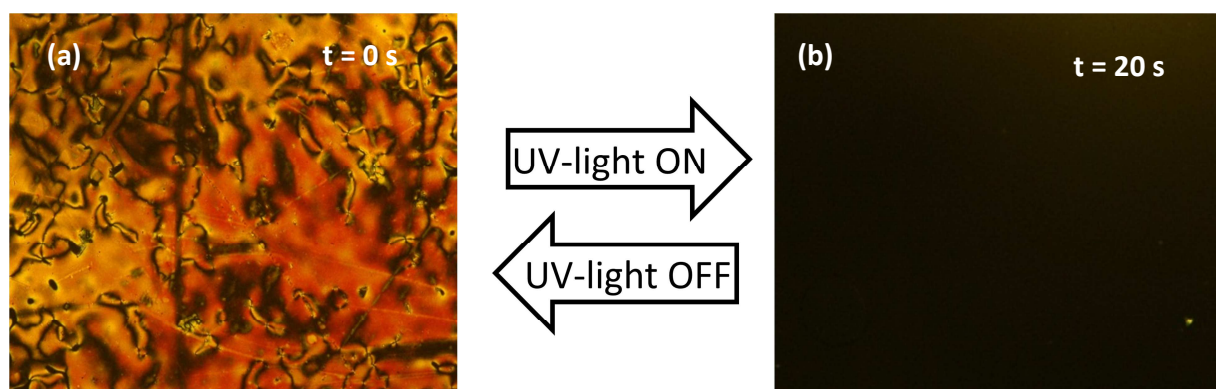


Fig 7. Change in the optical texture of the nematic phase on irradiation of the UV light (366 nm) at 119 °C in different time interval. (a) 0 sec; (b) 20 sec.

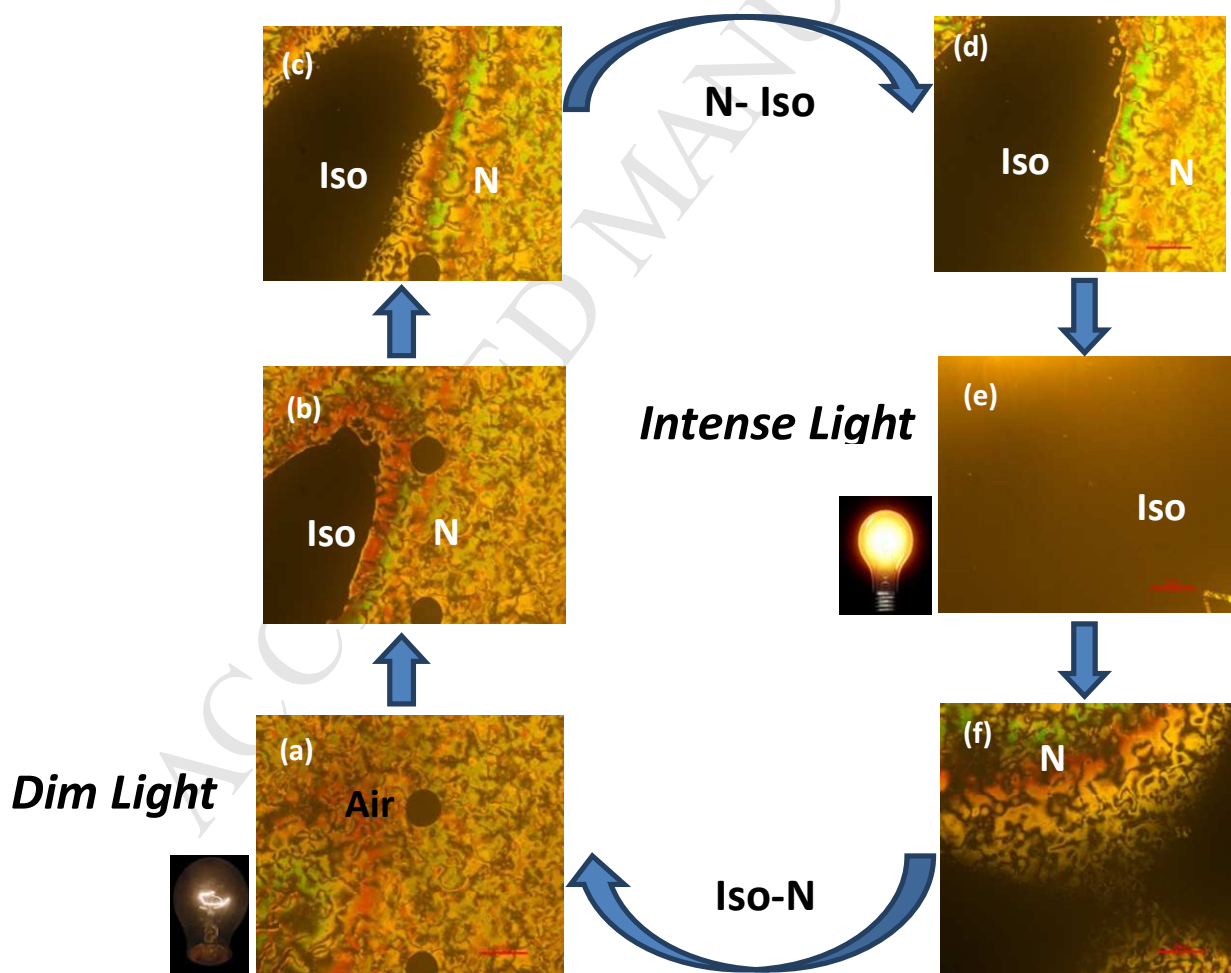


Fig 8. POM textures of the compound **5c** at constant temperature 119.5 °C on increasing the intensity of the halogen lamp light in a nematic phase: (a) Nematic phase; (b), (c) and (d) show isotropic region increase on increasing the intensity of the light; (e) isotropic liquid; (e) appearance of the schlieren texture of nematic phase.

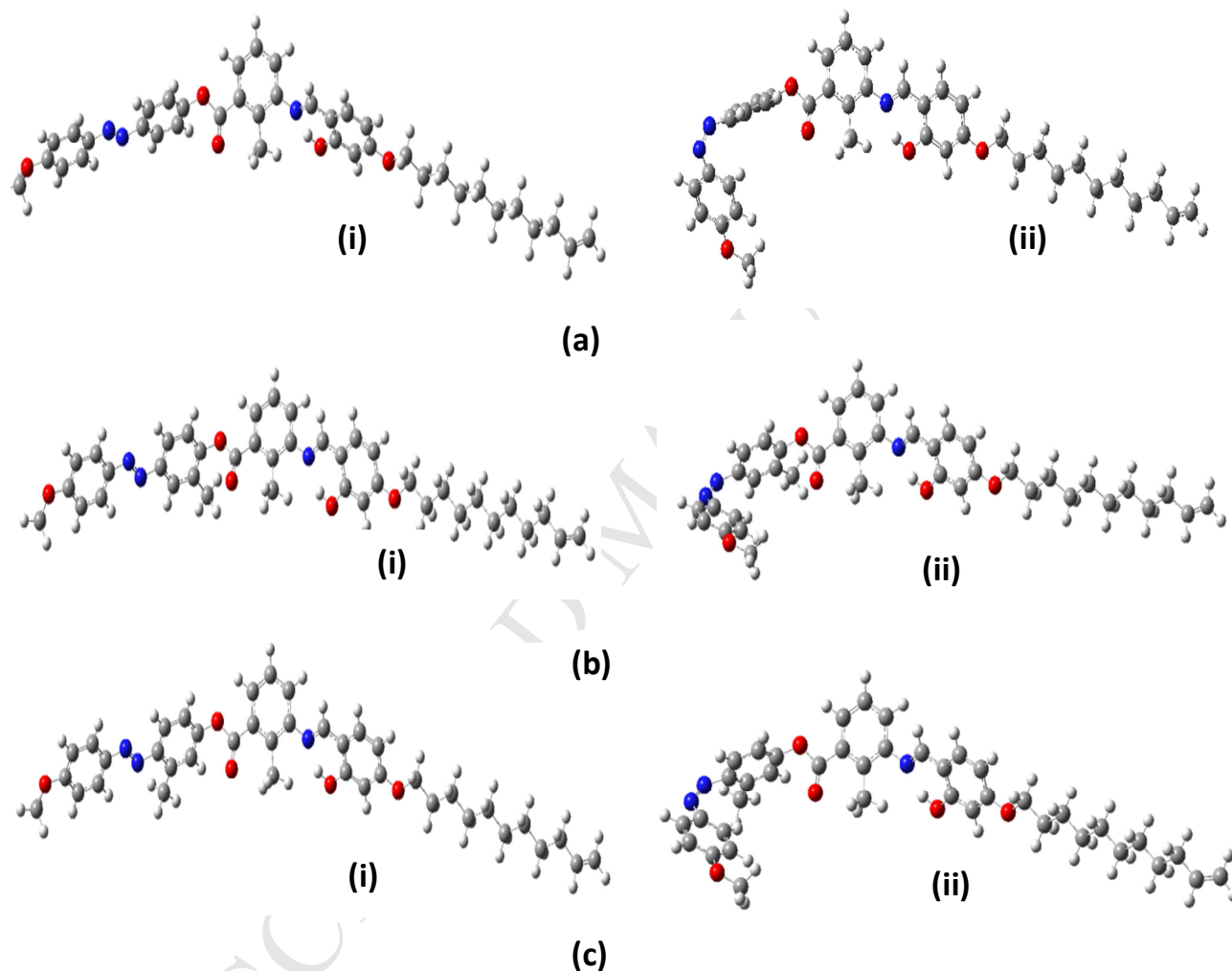
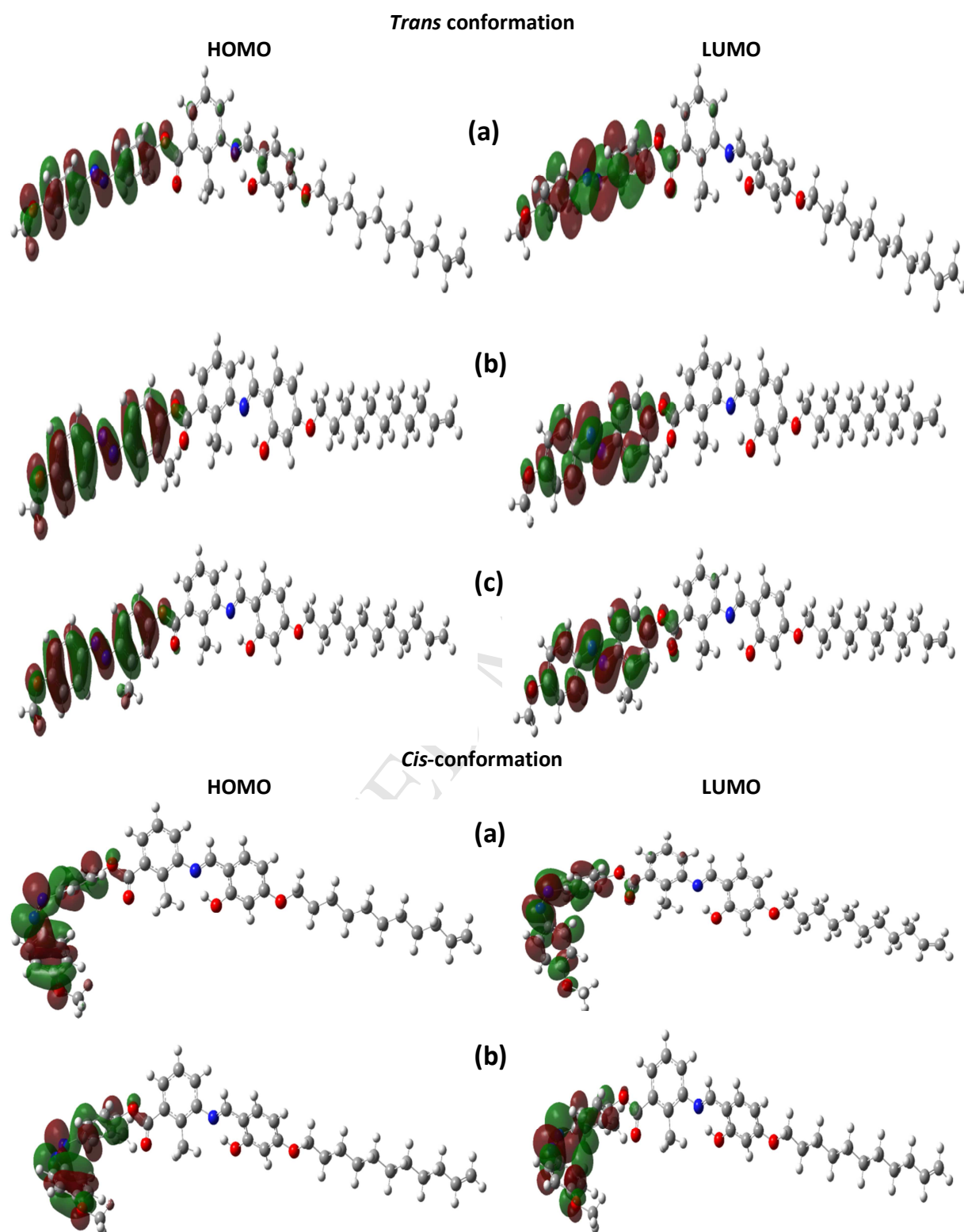


Fig. 9. Optimized geometry of hockey stick shaped mesogens compounds considering different positions of methyl group with respect to azo and /or ester group; (i) *trans* conformation (ii) *cis* conformation. (a) **5a**; (b) **5b**; (c) **5c**.



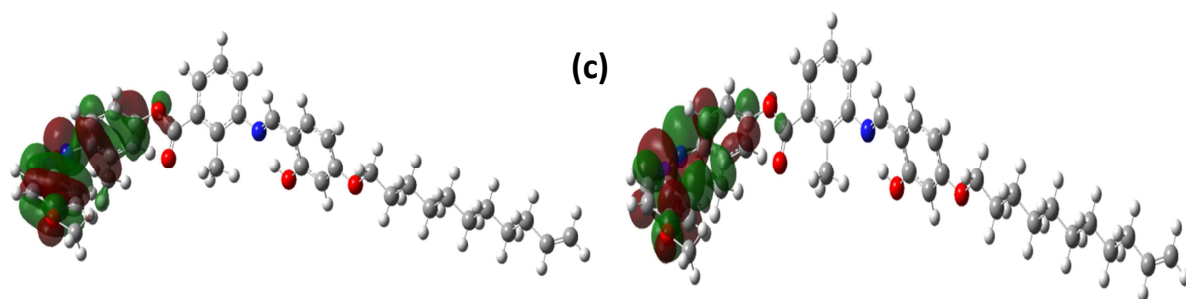


Fig. 10. Location of highest occupied molecular orbital (HOMO), lowest unoccupied molecular orbital (LUMO) of compounds (**5a-5c**) in solvent phase (a) **5a**; (b) **5b**; (c) **5c**.

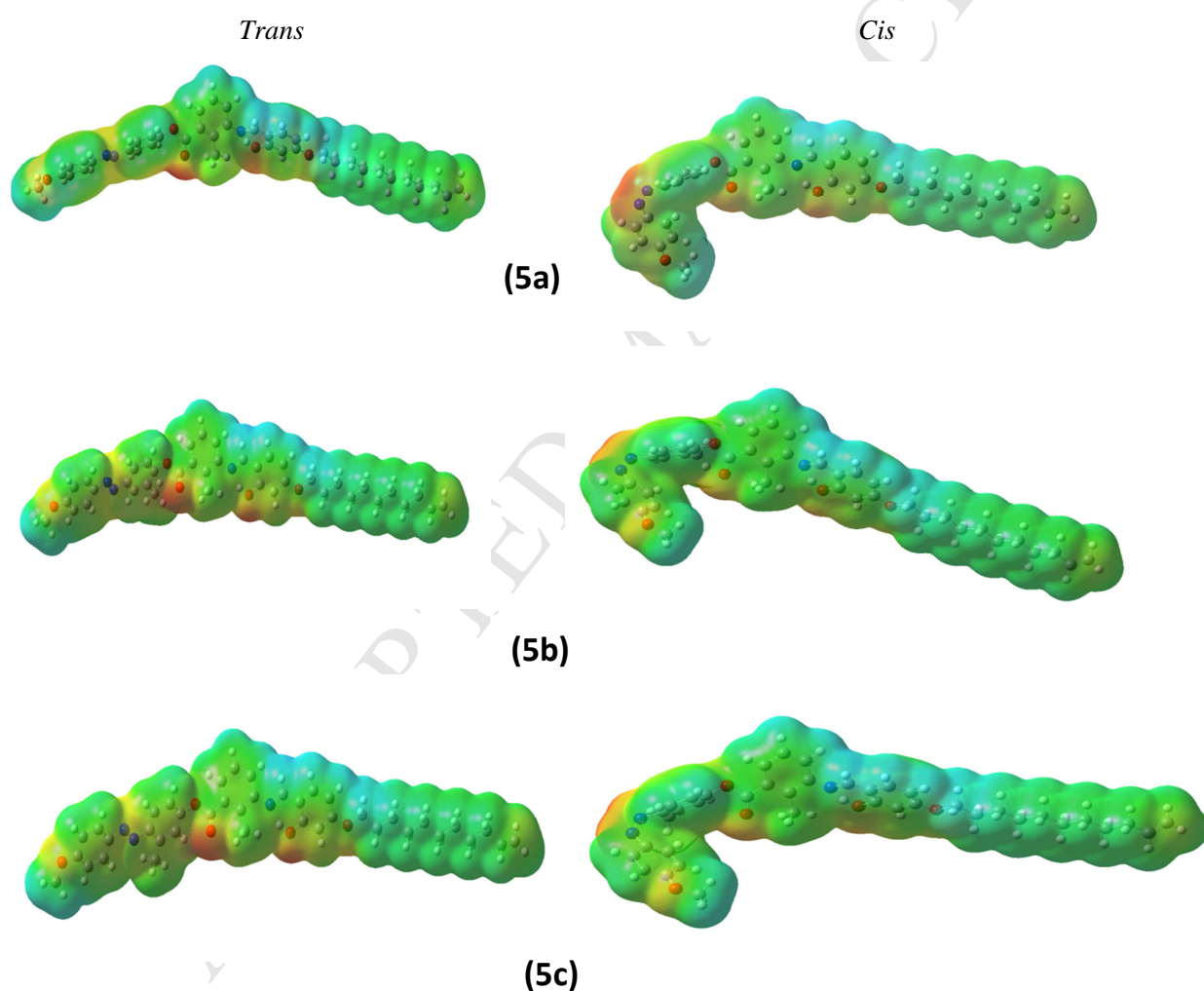


Fig. 11. The molecular electrostatic potential distribution of compounds (**5a-5c**) in solvent phase for both *trans* and *cis* conformations.

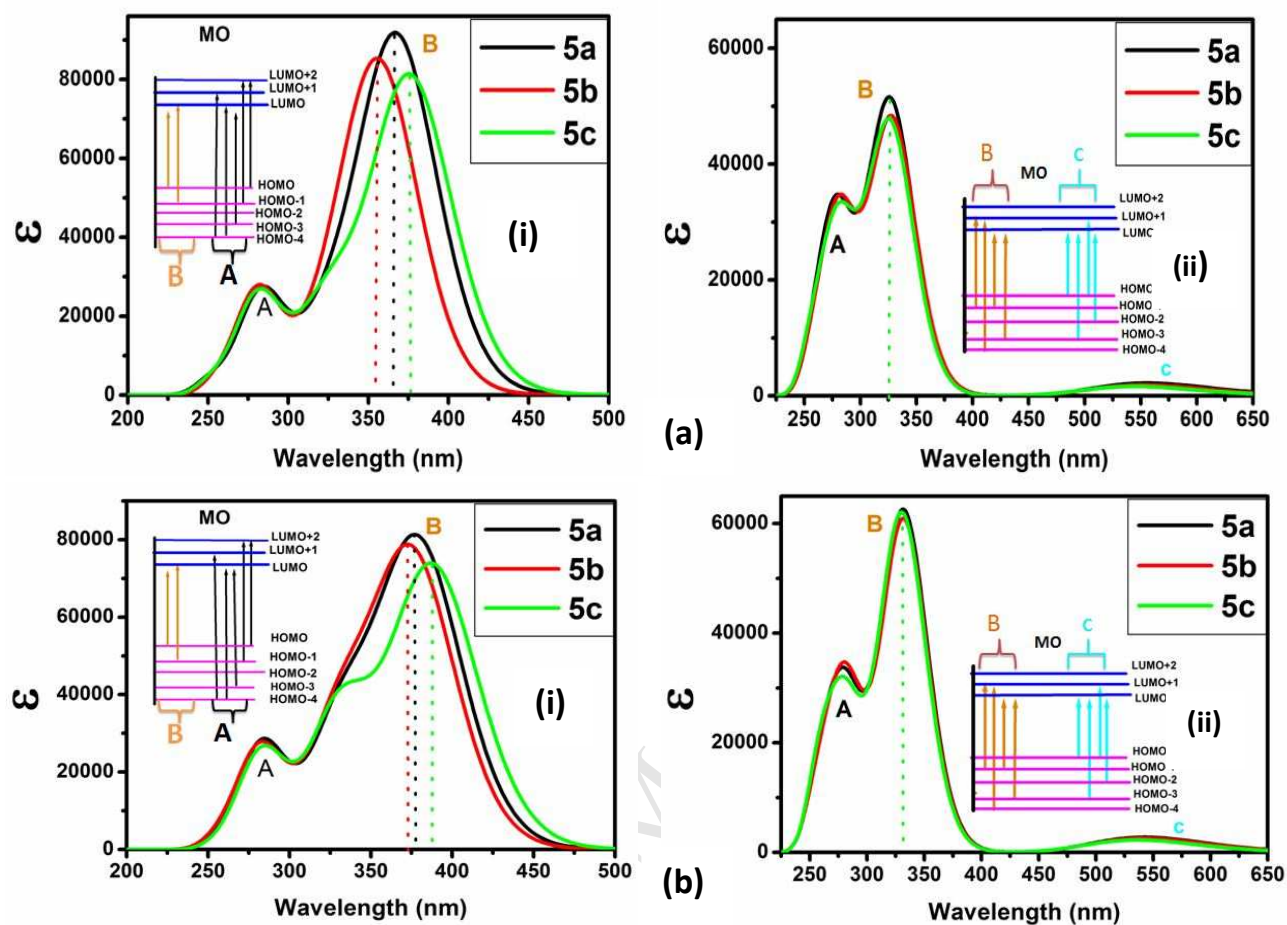


Fig. 12. UV-visible absorption spectra of compound (5a-5c) in (a) gas phase (b) solvent phase.

Here, (i) and (ii) represents the *trans* conformation and *cis* conformation respectively.

Highlights

- Design and synthesis of the new azo-functionalised reactive hockey stick mesogens.
- Compounds display low-temperature nematic phases.
- Photo-switching behaviour is observed in the nematic phase as well as in solution.
- Computational studies were performed to understand structural relaxation, spectroscopic properties and reactivity parameter of the azo-functionalised reactive hockey stick mesogens.